




Three-dimensional matrix stiffness-based stem cell soil: Tri-phase biomechanical structure promoted human dental pulp stem cells to achieve pulpodentin regeneration

Xiujuan Li^{a,1}, Yijing Xia^{a,1}, Zhiying Wang^{a,1}, Ziruo Yin^a, Maotao Weng^{b,c}, Feng Tian^a, Jie Kang^a, Yuanjiao Li^{a,d}, Peixuan Ding^a, Xing Liu^a, Bin Zhao^{a,*}, Lu Wang^{a,**} 

^a Shanxi Province Key Laboratory of Oral Diseases Prevention and New Materials, Shanxi Medical University School and Hospital of Stomatology, Taiyuan, 030001, Shanxi, China

^b Department of Thoracic Surgery, Guangdong Provincial People's Hospital, Guangdong Academy of Medical Sciences, Guangzhou, 510080, Guangdong, China

^c Shantou University Medical College, Shantou, 515041, Guangdong, China

^d Academy of Medical Sciences, Shanxi Medical University, China

ARTICLE INFO

Keywords:

Matrix stiffness
Three-dimensional culture
Paracrine signaling
Pulpodentin complex

ABSTRACT

The regeneration of the pulp-dentine complex is characterized by organizational diversity, with both dentine and pulp being essential for regenerating a complete tooth-like structure. Matrix stiffness plays a crucial role in guiding the multi-lineage differentiation of stem cells during the regeneration process. However, human dental pulp stem cell (HDPSCs) differentiation via three-dimensional (3D) matrix stiffness is still ambiguous. This study employed gelatin methacryloyl hydrogels of varying stiffness to investigate their effects on HDPSCs differentiation, and constructing a Tri-Phase Biomechanical Structure. The effects of 3D stiffness on HDPSCs proliferation, morphology, differentiation, and biomineralization were examined. The underlying mechanisms were analyzed by RNA sequencing (RNA-seq). At the same time, the comprehensive effects of 3D matrix stiffness-induced HDPSCs paracrine signals on periapical cells (endothelial cells, macrophages and fibroblasts) were evaluated. In vitro, high stiffness promoted dentin differentiation, medium stiffness supported vascular differentiation, and low stiffness enhanced vascularization of peri-apical cells through paracrine signals. In vivo, treated dentin matrixes implanted in nude mice further confirmed that this Tri-Phase Biomechanical Structure effectively promoted crownward dentin formation, pulp-like regeneration within root canals, and integration with peri-apical tissues. These findings highlight that understanding HDPSCs responses to 3D matrix stiffness is crucial for guiding targeted, efficient regeneration of a tooth-like pulpodentin complex.

1. Introduction

According to the World Health Organization, untreated permanent tooth decay is the most common oral disease of all epidemic diseases, with more than 2 billion cases worldwide [1,2]. In native teeth, the pulp cavity is surrounded by dentin to isolate external stimuli, and the pulp cavity is filled with vascularized connective pulp tissue. The pulp is the only soft tissue in the tooth and exchanges nutrients and nerve signals through the narrow apical foramen [3]. Once the continued development of caries causes pulp infection, the damage is usually irreversible and may further develop into pulp necrosis and periapical inflammation.

The pulp cavity and the periapical environment are connected, and the interruption of blood supply to the apex will lead to the loss of the pulp's conditions for clearing infection and repairing and regenerating [4,5]. Therefore, it is challenging and necessary to coordinate the regeneration of the pulpodentin complex while promoting apical vascularization [6–8].

Human dental pulp stem cells (HDPSCs) are very sensitive to the physical properties [9]. Liu et al. showed that high stiffness (18.23 ± 0.54 kPa) promoted HDPSCs osteogenic/odontogenic differentiation, while low stiffness (0.89 ± 0.43 kPa) regenerated pulp-like tissue [10]. These evidences indicate that regulating the precise differentiation of

* Corresponding author.

** Corresponding author.

E-mail addresses: sxmu0688@126.com (B. Zhao), wld02011@126.com (L. Wang).

¹ These authors contributed equally to this work.

HDPSCs by matrix stiffness may be a feasible strategy to achieve dental pulp regeneration. However, the current research on the effect of matrix stiffness on HDPSCs is still limited to two-dimensional (2D) culture [11], which is still different from the ECM in vivo. Cells living in a three-dimensional (3D) environment are closer to their natural state and are more similar to the body in terms of morphology and molecular regulation [12,13]. Regrettably, the impact of matrix stiffness on the fate of HDPSCs remains unclear when assessed within 3D environment. Therefore, this study further explored the regulatory effects of 3D matrix stiffness, which more closely mimics the natural in vivo environment and provides greater guiding significance for subsequent in-depth research.

During the integration of pulp regeneration and periapical tissue, another key point that we need to focus on is the paracrine signaling in stem cells, which may have complex effects on the proliferation, morphology, self-renewal and differentiation of surrounding cells [14–16]. For example, Wang et al. has shown that mesenchymal stem cells (MSCs) stimulated by soft matrix secrete higher levels of immunomodulatory factors, thereby promoting the differentiation of M2 macrophages [17]. Yet, how matrix stiffness affects the paracrine effects of HDPSCs has been little explored, which is of significant importance in determining the outcomes of stem cell-based pulpodentin tissue engineering and engineered tissue mimics. To date, the paracrine effects of dental pulp stem cells play a role in the regeneration of various soft and hard tissues, such as skull [18], blood vessels [19–21], nerves [22], macrophage polarization [23], salivary gland epithelium [24], etc. However, these studies still have many limitations. 1) no studies have been reported to investigate the paracrine effects of HDPSCs in response to matrix stiffness. 2) These studies have not determined the interaction between HDPSCs and periapical cells. Therefore, the paracrine signaling effect of HDPSCs in response to stiffness should be fully utilized. Paracrine signals can have synergistic or antagonistic effects on periapical cells, thereby affecting pulpodentin regeneration in the root canal.

We hypothesized that 3D matrix stiffness was a key biophysical cue that regulated HDPSCs differentiation and affected periapical tissues through paracrine signals of HDPSCs. Specifically, stiffness close to

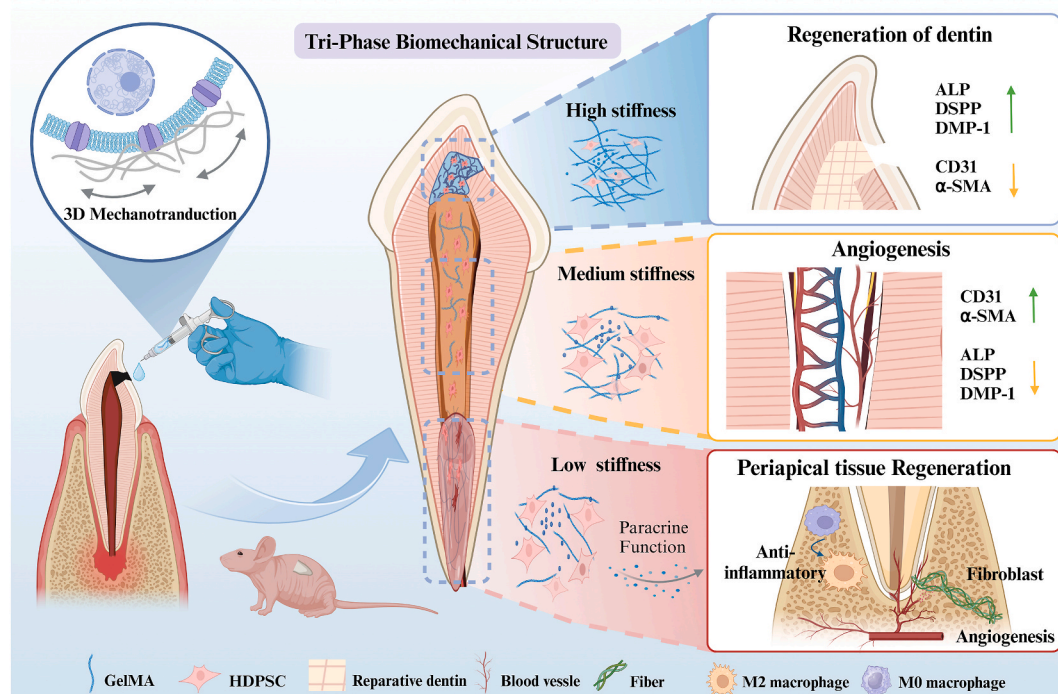
physiological dental pulp promoted HDPSCs to form soft pulp tissue, and harder stiffness promoted HDPSCs to form dentin. Softer stiffness was beneficial to the resolution of inflammation and promoted the growth of apical blood vessels and fibers through HDPSCs. HDPSCs were embedded in GelMA with different stiffness, and the effects of 3D stiffness on their proliferation, morphology, differentiation and biomineralization were examined, and the potential mechanisms were studied using transcriptome sequencing (RNA-seq) analysis. In addition, we evaluated the comprehensive effects of material stiffness-induced HDPSCs paracrine signals on periapical cells, including fibroblasts, endothelial cells, and macrophages. Finally, in order to coordinate the regeneration of the pulpodentin complex while promoting apical vascularization, and a semi-in situ dental pulp regeneration model was performed to verify the potential role of matrix stiffness in the formation of dental pulp tissue in vivo (Scheme 1). We envisioned that this unique construct would provide better adaptation to promote pulpodentin tissue regeneration and thus achieved excellent repair effects.

2. Materials and methods

2.1. Preparation and physical characterization of GelMA hydrogels

Preparation of GelMA hydrogel. According to previous reports [25], gelatin (Shanghai Maokang Biotechnology Co., Ltd., China) was stirred thoroughly in phosphate buffered saline (PBS, pH = 7.4) at 60 °C until completely dissolved. Methacrylic anhydride (Macklin, China) was dripped into the gelatin solution at a rate of 0.3 mL/min and then reacted at 50 °C in the dark for 3 h. To remove unreacted reactants, the supernatant was transferred to a dialysis bag after high-speed centrifugation. Dialysis was continued at 40 °C for 1 week, and then the final solution was freeze-dried and collected at −80 °C. Then, 3 %, 4 %, 5 %, 10 %, and 15% GelMA (w/v) solutions were dissolved in PBS and 0.1 % LAP was added to prepare hydrogels under 405 nm visible blue light irradiation for 10 s, 20 s, 30 s, or 40 s.

Mechanical testing. For mechanical property testing, GelMA hydrogels were prepared in Teflon molds (diameter = 15 mm, height =



Scheme 1. Schematic illustration of 3D matrix stiffness regulating the paracrine and regenerative functions of HDPSCs and promoting the regeneration of the pulpodentin complex. Created in BioRender.com.

10 mm) and irradiated as described above. All samples were measured at a compression rate of 1 mm/min until the sample strain reached 20 %. Young's modulus was obtained by partial linear regression of the stress-strain curves.

¹H NMR and FTIR analysis. Gelatin and GelMA were analyzed by FTIR (Nicolet is50, Thermo, USA) and NMR (AVANCE III 400, Bruker, Switzerland) in ATR mode. According to the NMR results, the degree of substitution of MA is calculated using the following formula:

$$\text{Methacrylation degree(\%)} = \frac{\text{Number of methacrylate groups}}{\text{Number of amine group on unreacted polymers}} \times 100$$

Sirius red staining. The hydrogel was cut into slices with a thickness of 20 μm by using a cry microtome, washed with running water for three times, and naturally dried at room temperature. The gelatin was stained by adding Sirius scarlet dye (Solarbio, China) for 8min, and observed under the optical microscope.

Degradation test. To measure the enzymatic degradation properties, the prepared High/Medium/Low GelMA hydrogel ($n = 3$ for each group) were immersed in 500 μL PBS containing 1U mL^{-1} collagenase type II at 37 $^{\circ}\text{C}$. At a predefined time, the samples were removed and washed with DI water to eliminate residual salts. After frozen and dried thoroughly, the weight of each sample was measured as W_2 , and the dry mass initially was W_1 . The degradation percent was calculated using the following equation: Degradation Percent = $(W_1 - W_2) / W_1 \times 100 \%$.

2.2. Cell culture

All cell types were cultured at 37 $^{\circ}\text{C}$ in a humidified atmosphere with 5 % CO_2 . Resuscitated HDPSCs (Tongpai Biotechnology, China) were cultured in a-modified essential medium (a-MEM) (Gibco, China) without ascorbic acid, supplemented with 10 % fetal bovine serum (FBS) (Gibco, USA) and 1 % penicillin-streptomycin (Penicillin-Streptomycin, P/S, Solarbio, China) in a humidified incubator at 37 $^{\circ}\text{C}$ with 5% CO_2 . The medium was changed every 2 days. Immortalized human dermal fibroblasts (HSF, iCell Bioscience Inc, Shanghai, China) were cultured in Dulbecco's Modified Eagles' Medium (DMEM)/F-12 Medium (Gibco, Carlsbad, CA) with a supplementary of 10 % FBS and 1 % P/S. Human umbilical vein endothelial cells (HUVECs, Tongpai Biotechnology, China) were cultured in high-glucose DMEM supplemented with 10 % FBS and 1 % P/S. Human THP-1 cells (iCell Bioscience Inc, Shanghai, China) were cultured in RPMI 1640 Medium (Gibco, Carlsbad, CA) with a supplementary of 10 % FBS and 1 % P/S. 100 ng/mL phorbol 12-myristate-13 acetate (PMA, Sigma, St. Louis, MO) was used to initiate the differentiation of THP-1 cells into THP-1 macrophages for 48h. The medium was changed every 2–3 days.

2.3. Seeding of HDPSCs within GelMA hydrogels

The cells cultured to P3 were digested with trypsin and collected by centrifugation, and resuspended in the hydrogel precursor solution after sterile filtration (0.22 μm filter membrane), and the cell density in the suspension was 1×10^6 cell/mL. The hydrogel suspension was placed in a cell culture dish and irradiated under 405 nm visible blue light for 20–30s, and HDPSCs were evenly embedded in the inductive gel. After the colloid was formed, DMEM complete medium was added, and cultured at 37 $^{\circ}\text{C}$ and 5% CO_2 , and the medium was replaced every 2 days.

2.4. Biocompatibility testing

Cell proliferation. Cell proliferation was assessed by CCK-8 (Solarbio, China). To investigate the direct inductive effect of stiffness on HDPSCs, HDPSCs were 3D-embedded in inductive gels and cultured with fresh growth medium for 1, 4, and 7 days. At the indicated time

points, they were washed three times with PBS and incubated in medium containing 10 % (v/v) CCK-8 for 1 h. After incubation at 37 $^{\circ}\text{C}$ for 1 h, the supernatant (100 μL) was removed from the wells and transferred to a new 96-well plate. The absorbance at 450 nm was measured using a microplate reader.

Cell viability. Cell viability was assessed by Live/Dead staining (Bestbio, China). In exploring the direct induction effect of stiffness on HDPSCs, HDPSCs were 3D-embedded in inductive gels and cultured with fresh growth medium for 1, 4, and 7 days. At the designated time points, they were washed three times with PBS at room temperature for 5 min each time. They were first incubated with diluted AM (labeled live cells, green) for 30 min, washed three times with PBS, 5 min each time, and then incubated with diluted PI (labeled dead cells, red) for 5 min, washed three times with PBS, 5 min each time. The images were observed and photographed using a laser confocal microscope. Excitation wave AM: Ex/Em490/515 nm; PI: Ex/Em535/617 nm).

2.5. Cytomorphology

Inverted microscope observation. HDPSCs were seeded in the inductive gel according to the above method, cultured in growth medium for 3 days, washed three times with PBS, and the morphology and distribution of cells inside the gel were observed under an inverted microscope.

F-actin staining. 2×10^5 HDPSCs were cultured in inductive gels of different stiffness for 3 days. Cell nucleus and F-actin were visualized by staining with 0.5 $\mu\text{g/mL}$ 4',6-diamidino-2-phenylindole (DAPI, Sigma-Aldrich, USA) for 5 min and phalloidin (A12379, Thermo Fisher Scientific, USA, 1:400) for 1 h at room temperature. The samples were washed three times with phosphate buffered saline (PBS, Servicebio, China). Then, the samples were observed using a confocal laser scanning microscope (FV3000, Olympus, Japan).

2.6. Odontogenic and angiogenesis induction of differentiation

Odontogenic induction of differentiation. Odontogenic-induced differentiation of HDPSCs was performed in medium supplemented with 10 mM sodium β -glycerophosphate (Sigma-Aldrich, China), 10 nM dexamethasone (Sigma-Aldrich, China) and 50 $\mu\text{g/mL}$ ascorbic acid (Sigma-Aldrich, China).

Angiogenesis induction of differentiation. The angiogenesis induction medium was EBM-2 medium (Lonza, USA) supplemented with 5 ng/mL VEGF, 5 ng/mL EGF, 5 ng/mL FGF, 15 ng/mL IGF-1, 10 mM glutamine, 0.75 units/mL heparin, 1 $\mu\text{g/mL}$ hydrocortisone, 50 $\mu\text{g/mL}$ ascorbic acid and 2%FBS. The medium was changed every 2 days and the test was performed after 14 consecutive days.

ALP quantitative experiment. In order to determine the viability of odontogenic differentiation, the supernatants extracted at 7 and 14 days of induction were quantified for ALP content by following the alkaline phosphatase detection kit (disodium phenyl phosphate microplate method).

Quantitative reverse transcription-polymerase Chain Reaction (RT-qPCR). On days 7 and 14 of growth, hydrogels were lysed using GelMA lysing solution (EFL, China), and cells were taken out to examine the expression of genes related to odontogenic differentiation and endothelial differentiation. Total RNA was extracted by column extraction (M5 Universal RNA Mini Kit, Mei5bio, China) according to the instructions in the operating manual. The first-strand complementary DNA (cDNA) was synthesized by reverse transcription using M5 Super qPCR RT Kit and gDNA Remover Synthesis Kit (Mei5bio, China). qPCR was then performed using an RT-qPCR system (Thermo Fisher Scientific), and the results were corrected using an internal reference gene. The primer sequences specific to the target gene and the internal reference gene used for RT-qPCR are listed in Table S1.

Immunofluorescence staining. Immunofluorescence staining was performed to observe odontogenic and angiogenesis. HDPSCs were

embedded in inductive gels at a density of 2×10^5 cells/mL, cultured in the odontogenic induction medium for 14 days, and stained for dentin sialoprotein phosphoprotein (DSPP). Cultured in the angiogenesis induction medium for 14 days, and stained for CD31. After washing, fixation, permeabilization and blocking, DSPP (rabbit source, 1:100, Abclonal) or CD31 (rabbit source, 1:100, Abcam) was used as the primary antibody, Alexa Fluor 488 was used as the secondary antibody, and DAPI was used to counterstain the cell nucleus.

2.7. Pure 3D stiffness induction of differentiation

3D Stiffness induction of differentiation. Cells of HDPSCs were embedded in inductive gels at a density of 1×10^6 cells/mL, cultured in the absence of induction medium for 7 and 14 days, and observed of the effect of 3D matrix directly inducing HDPSCs differentiation.

ALP staining. HDPSCs were embedded in inductive gels for 7 days. The qualitative ALP assay examined the odontogenic differentiation of HDPSCs using the pluripotent stem cell alkaline phosphatase chromogenic kit (Beyotime, China). The sample was observed and imaged using an optical inverted microscope. The average gray value of ALP staining (Int Den/Area) was measured using ImageJ software. Finally, the relative staining intensity relative to the low stiffness group was calculated.

ALP quantitative experiment. The method was the same as described above.

Conditioned medium(CM)collection from HDPSCs. To collect the paracrine products of HDPSCs in the inductive gel, HDPSCs were embedded in the inductive gel for 3 days, and the culture supernatant was collected and centrifuged at 2000 rpm for 10 min to remove dead cells and cell debris. The supernatant of the centrifugation solution was collected and stored at 4 °C before use. When used for cell culture, CM was mixed with complete growth medium at a ratio of 1:1.

Transwell migration assay. Because it was impossible to observe the migration of cells embedded in hydrogels, the previous method was used to collect CM to observe the cell migration ability [26]. 1×10^4 HDPSCs were inoculated into the upper compartment of the 24-well transwell plate. 300ul serum-free medium was added to the upper chamber and 500ul complete growth medium containing different CM was added to the lower chamber. 24 h later, the cell migration was observed.

Scratch test. Cell migration was assessed by scratch test. HDPSCs were seeded into 6-well plates and cultured to 90 % confluence with fresh growth medium. A 200ul pipette tip was used to scratch the center of the confluent cell monolayer and the floating cells were removed by rinsing twice with PBS. Subsequently, the cells were treated with growth medium containing different CMs for 0–36 h. Images were collected at 0 and 24 h by inverted microscopy. The healing area of the scratch wound and the initial scratch wound area were quantified using ImageJ software, and then the relative migration area to 0 h was determined. Finally, the relative migration area was calculated.

RT-qPCR. On days 7 and 14 of growth, hydrogels were lysed using GelMA lysing solution (EFL, China), and cells were taken out to examine the expression of genes related to odontogenic differentiation and endothelial differentiation. The method was the same as described above.

Immunofluorescence staining. Immunofluorescence staining was performed to observe odontogenic and angiogenesis. HDPSCs were embedded in inductive gels at a density of 2×10^5 cells/mL, without induction medium for 14 days, and stained for DSPP and CD31. The method was the same as described above.

2.8. RNA-seq and bioinformatics analysis

Cells of HDPSCs were embedded in different inducible gels and added to grow fresh growth media ($n = 3$ independent EU per group). After 7 days of culture, cells were collected. Total RNA was extracted by trizol reagent. The sequencing library was constructed and the gene

expression level was normalized by calculating Fragments Per Kilobase of exon model per Million mapped fragments (FPKM). For hierarchical cluster analysis and heat map generation, gene expression values are standardized by Z-scores between samples. After matching the identified genes, differentially expressed genes (DEG) with P value < 0.05 were identified, and further bioinformatic analysis was performed using gene ontology (GO) enrichment, Kyoto Encyclopedia of Genes and Genomes (KEGG) pathway enrichment and gene set enrichment analysis (GSEA).

2.9. Cell behavior under the action of paracrine factors (HUVECs, THP-1 macrophages and HSF)

In exploring the indirect induction effect of stiffness on apical pericytes through the paracrine products of HDPSCs, HUVECs, THP-1 macrophages and HSF were seeded into 24-well plates and cultured in growth medium containing CMs for 1 and 3 days.

Cell proliferation. Cell proliferation was assessed by CCK-8. The method was the same as described above.

Cell viability. Cell viability was assessed by Live staining. The method was the same as described above.

Transwell migration assay. 1×10^4 HUVECs cells were inoculated into the upper compartment of the 24-well transwell plate. 300ul serum-free medium was added to the upper chamber and 500ul complete growth medium containing different CM was added to the lower chamber. 24 h later, the cell migration was observed.

Scratch test. HUVECs and HSF migration was assessed by scratch test. The method was the same as described above.

Flow cytometry. Following a 48-h incubation period with PMA, the THP-1 cells were separated by centrifugation, subjected to two rounds of cold PBS washing, and stained using anti-CD11b antibodies (Invitrogen, USA) labeled with PE. Utilizing flow cytometry (Agilent, USA), the proportion of macrophages was determined.

RT-qPCR. On days 3 of growth, HUVECs were taken out to examine the expression of genes related to endothelial differentiation. On days 1 and 3 of growth, THP-1 macrophages were taken out to examine the expression of genes related to macrophage polarization. The method was the same as described above.

Immunofluorescence staining. HUVECs cells were seeded in 24-well plates at a density of 1×10^4 cells/mL, cultured with different CMs from HDPSCs for 3 days, and stained for CD31. THP-1 macrophages cells were seeded in 24-well plates at a density of 1×10^4 cells/mL, cultured with different CMs from HDPSCs for 3 days, and stained for CD86 and CD206. HSF cells were seeded in 24-well plates at a density of 1×10^4 cells/mL, cultured with different CMs from HDPSCs for 3 days, and stained for VEGF. The method was the same as described above.

2.10. In vivo experiment

Preparation of treated dentin matrixes (TDM). TDM was prepared using a more mature method that has been published [27]. After being reviewed and approved by Shanxi Stomatology Ethics Committee (the ethical approval number: 2024SLL040) and with the informed consent of the patient, we collected complete single canal premolars that needed to be removed for clinical orthodontic treatment, requiring complete roots without caries, cracks and filling bodies. The freshly extracted single tooth was repeatedly rinsed with PBS buffer and immersed in PBS solution with 1 % double antibody (stored at -20°C for later use). The crown (enamel dentin boundary) and root tip (2 mm) of the isolated teeth were truncated with a high-speed dental turbine, the pulp was removed completely with a pulp pulling needle, the remaining periodontal tissue was scraped with a sterile surgical blade, and the internal pulp and part of the dentin, as well as the external periodontal membrane and cementum were removed. The shape was further trimmed and short dentine segments with a length of 4–5 mm were made to meet the transplantation requirements. A nickel-titanium rotary instrument prepared the root canal to Protaper25#, alternating a large dose of 5.25%

NaClO with 17%EDTA for each instrument change. The resulting human dentin matrix was then soaked in deionized water for 5 h and mechanically cleaned with an ultrasonic cleaning machine for 20 min every hour. The deionized water was changed every hour. The cleaned dentin scaffold material was placed in 100 mL wide-mouthed bottle containing EDTA of different concentrations, and the wide-mouthed bottle was placed on a magnetic stirrer for stirring demineralization in the following order: the RS were immersed in EDTA (17 %) for 5 min, followed by a 10 min rinse in deionized water, and a final 10 min soak in EDTA (5 %) before another 10 min rinse in deionized water, finally obtained TDM. TDM was immersed in sterile PBS containing penicillin (100 U mL^{-1}) and streptomycin ($100 \mu\text{g mL}^{-1}$) for 3 days and rinsed in sterile deionized water for 10 min. Finally, TDM were stored in DMEM at 4°C .

Subcutaneous implantation in nude mice. Eighteen treated tooth root segments were selected and randomly divided into three groups, with 6 samples in each group. The groups were Blank, Medium and Tripartite. Nine healthy male BALB/c Nude mice aged 6–8 weeks were selected and randomly divided into three groups, with 3 mice in each group. After the BALB/c Nude mice were anesthetized by isoflurane inhalation, the back of the mice was cleaned with iodine wipes. Under sterile conditions, a longitudinal incision of about 1 cm in length was made in the middle and lower part of the back of the nude mice. The subcutaneous tissue on both sides of the incision was bluntly separated, and the samples were implanted, one on each side of each nude mouse. The incision was sutured and the complex was disinfected with iodine. Toxic skin. After surgery, the nude mice were closely observed until they woke up and breathed normally, and then they were returned to the animal cage for continued feeding (Fig. S6). Eight weeks after transplantation, the implanted samples were removed and immersed in 4 % paraformaldehyde for 48 h. The samples were then demineralized in 10 % EDTA solution for 4 weeks, and the demineralization solution was changed every three days. After demineralization was completed, the samples were dehydrated, embedded and sliced. Each specimen was longitudinally sliced into paraffin sections with a thickness of $5 \mu\text{m}$, and histological analysis was performed by hematoxylin-eosin (HE) staining, Masson trichrome staining, and immunohistochemistry.

Hemolysis test. To evaluate the blood compatibility of the hydrogel, fresh blood from BALB/nude mice and sodium citrate (3.8 wt%) were mixed in a ratio of 9:1 and diluted with saline (volume ratio of 4:5). The samples were soaked in 10 mL saline test tubes and kept at 37°C for 30 min. Then, 0.2 mL of diluted blood was added to each test tube, and the mixture was incubated at 37°C for 60 min. 10 mL of saline solution was used as a negative control, and 10 mL of deionized water was used as a positive control. Then, centrifugation was performed at 3000 rpm for 5 min. The optical density (OD) of the clear supernatant was detected at a wavelength of 542 nm using a spectrophotometer. The hemolysis rate was expressed as a percentage and calculated using the following formula:

$$\text{HR} = [\text{ODt} - \text{ODn}] / [\text{ODp} - \text{ODn}] \times 100\%$$

where HR was the haemolysis ratio (%); ODt was the OD value of the tested group; ODn was the OD value of the negative control; ODp was the OD value of the positive control.

HE staining. Allowed observation of cellular morphology of new tissues and internal organs by light microscopy. HE staining was performed using a biological tissue intelligent automatic staining machine. The staining steps were to place the slices in xylene and ethanol for dehydration and dewaxing, and then stain the slices with hematoxylin and eosin staining solution. Then rinsed, dehydrated and permeabilized, and finally sealed with gum and observed under a microscope.

Masson staining. The tissue sections were fixed on glass slides, the nuclei were stained with hematoxylin to make them blue, and then the collagen fibers were stained with acid fuchsin to make them red. Finally, the sections were dehydrated, made transparent, and sealed.

Histological analysis. The slices were soaked in xylene solution and ethanol solutions of different concentrations for different periods of time. After completion, the slices were heated in a microwave oven to repair the antigens. Next, the slices were soaked in 3 % hydrogen peroxide and then cleaned. Goat serum was dripped on each slice for antigen blocking. After blocking, the diluted primary antibody was dripped, and then the slices were placed in a wet box at 4°C overnight. After that, the primary antibody was rinsed with PBS, and then the secondary antibody was dripped, incubated at 37°C for 30 min, and then DAB solution was dripped for color development and hematoxylin staining was used to counterstain the cell nucleus. Routine dehydration and sealing operations were performed, and then the antibody expression was observed under a microscope.

2.11. Statistical analysis

In this study, a minimum of three independent replicates were set up for each experimental group to ensure the reliability and repeatability of the data. The results were presented as mean \pm standard deviation (Mean \pm SD). Statistical differences between experimental groups were assessed using one-way analysis of variance (ANOVA) with GraphPad Prism 9.0 software. A p-value <0.05 was considered statistically significant.

3. Results

3.1. Preparation and characterization of hydrogels with various stiffness

We prepared GelMA by reacting gelatin and MA, as shown in Fig. 1A, to study how matrix stiffness affects the behavior of HDPSCs. Previous studies had shown that using gelatin as a research platform for three-dimensional matrix stiffness can effectively exclude the profound effects of matrix viscoelasticity, RGD density, and network permeability on cell behavior [17]. Different concentrations of gelatin could provide a high degree of freedom in controlling matrix stiffness. The chemical structures of gelatin and GelMA were analyzed by FTIR and ^1H NMR. As shown in Fig. 1B, the characteristic peak of amide was observed at 1620 cm^{-1} . The stretching vibration peak of the -OH group or the stretching vibration peak of NsH was simultaneously observed at 3270 cm^{-1} . At the same time, the peaks at 1535 cm^{-1} and 1440 cm^{-1} , respectively, the peak at 2920 cm^{-1} was the bending vibration of N-H and C-H, and the peak at 2920 cm^{-1} was the stretching vibration of C-H. These results indicated that the peaks in the FTIR spectrum correspond to the characteristic functional groups of GelMA [28]. In addition, the ^1H NMR spectrum should be used to confirm the modification of gelatin by MA. As shown in Fig. 1C, due to the numerous amino acids and peptides found in both gelatin and GelMA, complex ^1H NMR spectra were seen. Notably, the methacrylate of gelatin was successfully achieved, which was confirmed by the appearance of methyl ($\delta = 1.9 \text{ ppm}$) and vinyl proton ($\delta = 5.4/5.7 \text{ ppm}$) signals and the decrease in the intensity of lysine signal ($\delta = 2.99 \text{ ppm}$). According to the ^1H NMR results, the degree of methacrylate was about 61.68 %. Fig. 1D was a representative image of the prepared GelMA, which is spongy after freeze-drying. Next, the compression modulus of each group was measured by a universal mechanical tester (Fig. 1E). The results were shown in Fig. 1F. With the increase of GelMA content and the extension of irradiation time, the stiffness of the hydrogel increased from 0.22 kPa to 60.34 kPa (Fig. 1G). Studie has shown that the compression modulus of physiological pulp is $5.5 \pm 2.8 \text{ kPa}$ [29]. Therefore, this study selected compression moduli of 0.79 kPa (low stiffness), 6.37 kPa (medium stiffness) and 24.12 kPa (high stiffness) as stiffness gradient induced gels (Fig. 1H). The frozen sections can restore the real pore structure of the hydrogel to the greatest extent by instantaneous freezing fixation [30]. As illustrated in Fig. 1H, the gradient stiffness-inductive hydrogel exhibited a highly porous structure, which facilitated the essential nutrient exchange for cells. Additionally, the degradation behavior is a critical property of tissue

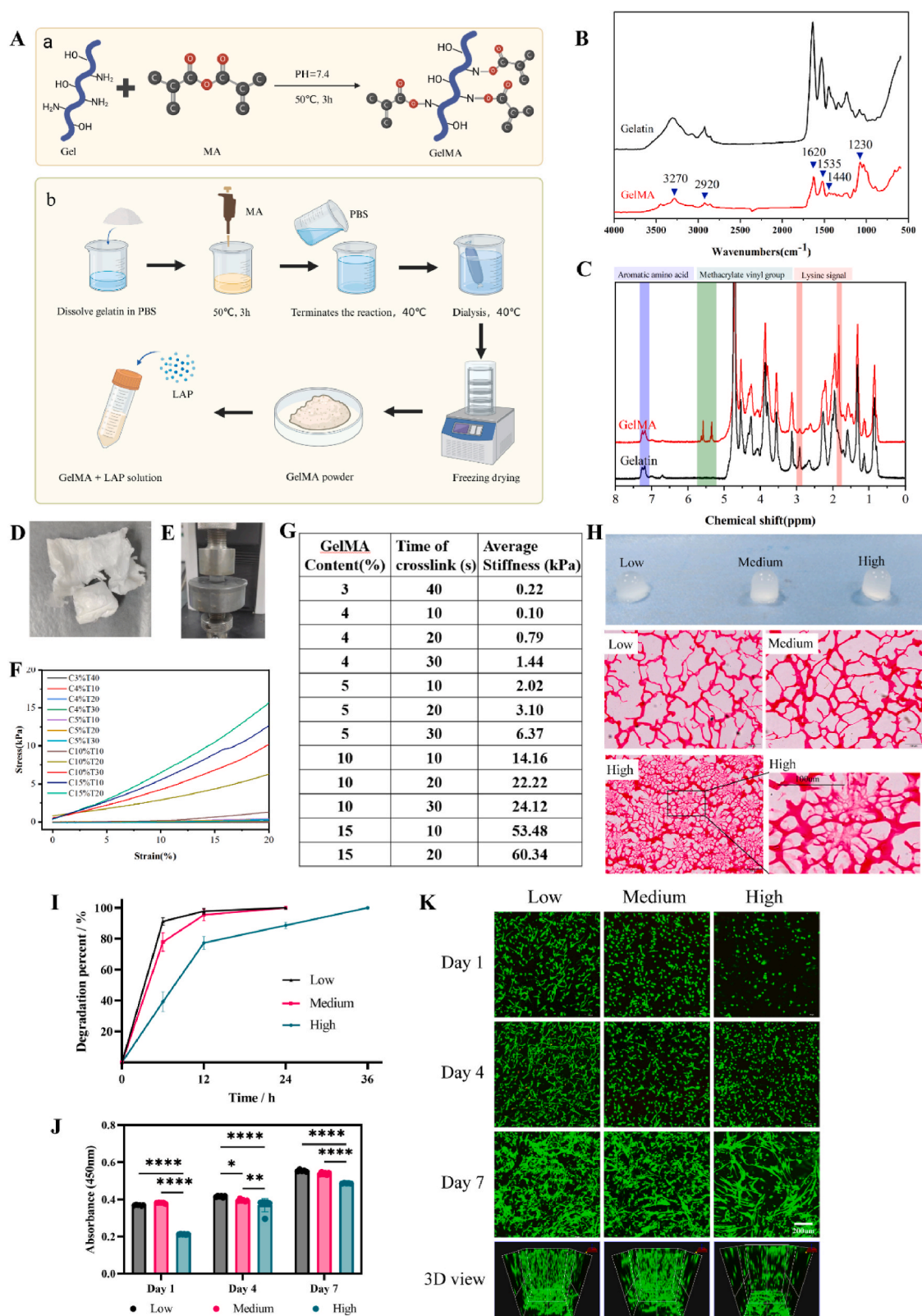


Fig. 1. Characterization of gels with different stiffness. A) Preparation scheme of GelMA hydrogel crosslinked by visible light. B) FTIR analysis of chemical structures of gelatin and GelMA. C) ^1H NMR(D_2O) spectra of gelatin and GelMA. D) Sponge GelMA after freeze-drying. E) Measurement method of gel compression mechanics. F) Typical compressive stress-strain curve, C and T represent GelMA content and crosslinking time, respectively. G) GelMA composition, crosslinking time and average stiffness of each group. H) Above: representative macro images of gels with different stiffness. Below: representative frozen section images of gels with different stiffness. Scale bar = 100 μm . I) Degradation percent of GelMA. J) Cell viability was measured by CCK-8 method ($n = 3$). K) Live/dead staining of HDPSCs inoculated in hydrogel showed that the cells in each group were evenly distributed. There were few dead cells. Results are presented as mean \pm SD (standard deviation). Statistical significance: * $P < 0.05$, ** $P < 0.01$, *** $P < 0.001$. One-way ANOVA followed by Tukey's post hoc tests.

engineering materials. The biodegradability of hydrogels with high, medium, and low stiffness is illustrated in Fig. 1I. GelMA was fully degraded within 36 h when incubated with collagenase II. In order to study the cell compatibility of hydrogels with various matrix stiffness, HDPSCs were embedded in hydrogels with different stiffness for 1, 4 and 7 days. Live-dead double staining technique was used to observe cell proliferation and morphology under a laser confocal microscope. The live/dead staining results showed that all HDPSCs cells were stretched in the gel, survived well and were evenly distributed, and the cells in the copolymer gel proliferated significantly over time (Fig. 1K). The cells in the high stiffness group hydrogel were slightly sparse, but the CCK-8 results on the 1st, 4th and 7th days showed that the cells in all hydrogel groups maintained high metabolic activity (Fig. 1J).

3.2. Matrix stiffness affected the shape of HDPSCs

Three days after cell seeding, HDPSCs migrated within GelMA of different stiffnesses and appeared in different morphologies. Direct observation of HDPSCs encapsulated in matrix revealed that the cells in the low stiffness showed obvious elongated shape, and the connections between cells were tightly intertwined into a network. While the cells in the high stiffness were spherical, with cells dispersed independently of each other (Fig. 2A). The results of phalloidin staining were further confirmed (Fig. 2A), the HDPSCs in the low stiffness had slender cell bodies, many and long pseudopods. When the cells are embedded in a medium stiffness matrix, the cells were still slender, but the number of pseudopods was reduced and the length was shortened. When the cells

were embedded in a high stiffness matrix, the cells were overall spherical, the cell body was round and extended, and the pseudopodia were very small. This was significantly different from the morphology of HDPSCs cultured on 2D under different stiffnesses. The HDPSCs on the hard matrix showed cell spreading and increased pseudopodia, while the HDPSCs on the soft matrix remained cells separated from each other [31]. This further proved diverse behavior of HDPSCs in 2D and 3D and indicated the necessity to investigate HDPSCs functions in 3D which is of more relevant in clinical applications. Quantitative analysis of cell area (S) showed that HDPSCs in low stiffness had a higher area ($S = 3153.6745 \pm 123.3633 \mu\text{m}^2$) than HDPSCs in medium and high stiffness (Fig. 2B). In addition, the aspect ratio (γ) of HDPSCs in low stiffness was 4.5 ± 0.2 , which was significantly higher than that of medium stiffness ($\gamma = 3.7 \pm 0.1$) and high stiffness ($\gamma = 1.7 \pm 0.1$) (Fig. 2C). These results confirmed the mechanical transduction of HDPSCs on matrix stiffness and GelMA hydrogels developed here can be utilized as a good model as mechanical cues to study the effect of stiffness on HDPSCs behavior and its paracrine effects.

3.3. Stiffness directly regulated the differentiation of HDPSCs

3D matrix stiffness synergized lineage specification of HDPSCs. In order to explore whether the 3D matrix stiffness affected the differentiation of HDPSCs under chemical induction conditions. Ensured that all groups were in the chemical induction environment of osteogenic induction solution, HDPSCs were embedded in hydrogels with different matrix stiffness and cultured for 7 days and 14 days, and then detected

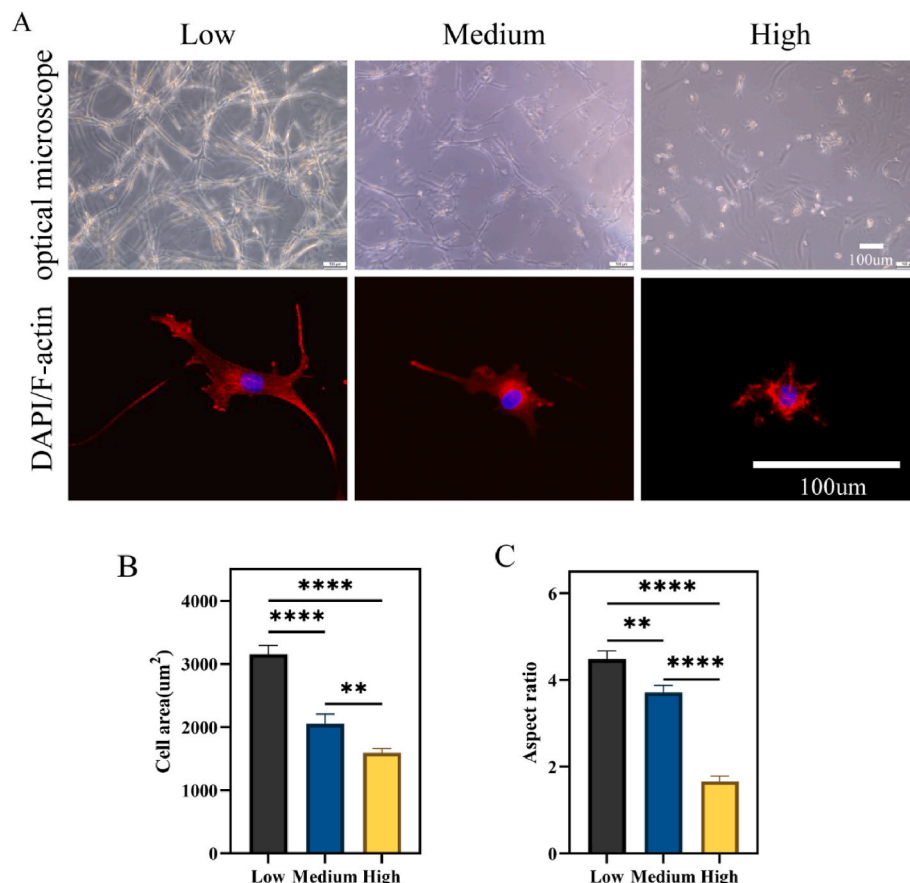


Fig. 2. The morphology of HDPSCs in GelMA matrices of different stiffness. A) The morphology of HDPSCs cultured in 3D hydrogel for 3 days. And F-actin immunofluorescence staining (red) and DAPI immunofluorescence staining (blue) of HDPSCs coated with different GelMA substrates (scale = 100 μm, n = 4). Quantification of the projected B) cell area and C) cell aspect ratio. Results are presented as mean ± SD. Statistical significance: *P < 0.05, **P < 0.01, ***p < 0.001, ****p < 0.0001. Tukey back testing was used after one-way analysis of variance. (For interpretation of the references to color in this figure legend, the reader is referred to the Web version of this article.)

the expression of odontoblast markers. The results of the quantitative ALP showed that there were significant differences in the expression of ALP in each group. The high stiffness had the highest alkaline phosphorus enzyme activity on days 7 and 14 (Fig. 3A). Similarly, the HDPSCs, cultured in high stiffness, had the highest mRNA expression levels of DSPP and dentin matrix acidic phosphoprotein 1(DMP-1) ($P < 0.05$) (Fig. 3B and C). We observed the immunofluorescence staining of odontogenic marker DSPP in hydrogel-cultured HDPSCs after 7 days. Under the same chemical induction conditions, the odontogenic differentiation of the high stiffness was enhanced, compared with the other two groups (Fig. 3D and E). These results showed that, three-dimensional matrix stiffness played an important role in the chemical induction process of odontoblast, while high stiffness played a synergistic role in the chemical induction process of odontoblast. In dental pulp regeneration, vascular regeneration was another important indicator to measure the regeneration effect [32]. HDPSCs were subjected to vascular chemical induction at the same time, and all groups could express vascular markers. However, the three-dimensional matrix stiffness significantly affected the expression of vascular markers in HDPSCs. After 14 days of induction, the mRNA expression level of CD31 and α -SMA was significantly higher than that in the low stiffness and high stiffness groups (Fig. 3F and G). The CD31 protein expression level also had the same trend after culturing HDPSCs for 14 days. The immunofluorescence quantitative results showed that CD31 protein expression level in the medium stiffness group was significantly higher than the other two groups (Fig. 3H and I). All above results showed that medium stiffness cooperated with chemical induction reagents to promote the angiogenesis of HDPSCs. In summary, the "correct" 3D matrix stiffness could cooperate with chemical induction reagents to promote better differentiation effect of HDPSCs.

3D matrix stiffness directed lineage specification of HDPSCs.

Studies had shown that matrix stiffness guides lineage specification of stem cells [28,33]. Matrix stiffness influences stem cell lineage specification via focal adhesion-actin-myosin contraction, even in the absence of chemical inducers [33]. We evaluated the effect of hydrogel stiffness alone on the differentiation of HDPSCs. HDPSCs were respectively embedded in different stiffnesses for lineage induction, without adding any chemical inducer to evaluate the effect of matrix stiffness on the differentiation of HDPSCs into dentin and endothelium. The production of alkaline phosphatase marked the beginning of the mineralization process. Crucially, it was beneficial to the formation of tertiary dentin [34]. As shown in Fig. 4A, the high stiffness had the deepest alkaline phosphatase staining. ALP semi-quantitative results (Fig. 4B) and ALP quantitative experiments (Fig. 4C) both showed that the expression of alkaline phosphatase in the high stiffness was significantly higher than that in the low stiffness. To further explore the effect of 3D matrix stiffness on the differentiation of HDPSCs into odontoblasts, RT-qPCR was used to analyze odontoblast markers genes DSPP and DMP-1 (Fig. 4D and E). The results showed that the expression of the two detected tooth-related genes in each group showed an overall upward trend. The mRNA expression level of the high stiffness was significantly higher than the other two groups at 14 days. However, when matrix stiffness was induced for 7 days, there was no significant difference in the mRNA expression between the groups. This might be because pure matrix stiffness required a long enough induction time to guide the lineage specification of HDPSCs [33]. After 14 days of culture, the DSPP protein expression level of HDPSCs showed that the high stiffness was significantly higher than the other two groups (Fig. 4F and G), and the trend of the results was consistent with mRNA. Further, we explored the vascular differentiation of HDPSCs. The increase in cell migration ability was usually related to angiogenesis. First, we tested the migration ability of HDPSCs in the three-dimensional matrix stiffness. Compared with the high stiffness, the transwell of the low and medium stiffness showed the migration number of HDPSCs increased. And the medium stiffness was significantly higher than the high one (Fig. 5C and E). The scratch assay also confirmed that the migration number of HDPSCs in the medium

stiffness had the highest closure rate (Fig. 5A and B). And then, we detected the expression levels of angiogenesis-related genes CD31 and α -SMA. The RT-qPCR results showed that at 7 and 14 days, the medium stiffness had the highest expression levels (Fig. 5F and G). Similarly, at the protein level, we used immunofluorescence staining to detect the expression of the endothelial cell surface marker CD31 at 14 days. As shown in Fig. 5D and H, there was almost no expression of fluorescent markers in the high stiffness, while the expression of CD31 in the medium stiffness increased significantly. This suggested that medium stiffness had the highest possibility of vascular differentiation. It provided the possibility for dental pulp regeneration in vivo. Above all, the three-dimensional matrix stiffness played an important role in regulating the differentiation of HDPSCs. Three-dimensional matrix stiffness could direct lineage specification of HDPSCs.

3.4. Widespread transcriptomic alterations triggered by 3D matrix stiffness

HDPSCs induced by different three-dimensional matrix stiffness showed significant differentiation differences. In this study, RNA-seq was used to conduct in-depth analysis of the transcription profiles of HDPSCs under high, medium, and low stiffness, in order to explore the influence of 3D matrix stiffness on the transcription regulation of HDPSCs. In the experiment, HDPSCs were cultured in different matrix stiffness for 7 days, and the gene expression level was standardized using Fragments Per Kilobase of exon model per Million mapped fragments (FPKM) method. Supervised partial least squares discriminant analysis (Plsda) was used to evaluate the correlation between the samples. And the results showed that the inter-group samples showed a clear tendency to disperse, while the intra-group samples were basically clustered (Fig. S1). Further pair-to-pair comparative analysis revealed differentially expressed genes (DEGs) in HDPSCs treated with different matrix stiffness. Specifically, compared with the low stiffness group, 223 genes were up-regulated and 518 genes were down-regulated in the high stiffness group (Fig. 6A). Compared with the high stiffness group, 507 genes were significantly up-regulated and 417 genes were significantly down-regulated (Fig. 7A). The differences between the medium stiffness and high stiffness were relatively small, with only 72 genes up-regulated and 160 genes down-regulated (Fig. S2). These results suggested that changes in three-dimensional matrix stiffness significantly affected the cellular response of HDPSCs.

In vitro experiments on odontogenic related indicators, the difference between high stiffness and low stiffness was the most significant. Therefore, this study further analyzed the differential gene expression between the two groups to explore the effect of 3D matrix stiffness on the expression of odontoblast-related genes. Similarly, in vitro experiments on angiogenesis related indicators, the difference between the medium and high stiffness groups was the most significant, which was consistent with the expression trend of DEGs. Therefore, the present study also analyzed the differential gene expression between the two groups to explore the effect of three-dimensional matrix stiffness on the expression of genes associated with angiogenesis.

The ability of HDPSCs to differentiate into odontoblast cells was a key indicator of pulpodentin complex regeneration. In this study, the gene expression levels of HDPSCs in high stiffness and low stiffness groups were analyzed. Pair-to-pair comparisons showed that the low stiffness group had 2845 unique DEGs, while the high stiffness group had 2809 unique DEGs (Fig. 6B). Cluster heat map analysis was used to visualize the odontogenic associated DEGs within each group (Fig. S3A). Gene ontology (GO) annotation and functional analysis suggested that, compared to the control group, the upregulated DEGs in the high stiffness group exhibited significantly increased expression, particularly genes related to collagen fibril organization, extracellular matrix organization, odontogenesis, and bone mineralization (Fig. 6C), which further verified the results of this study. In addition, genes related to bone mineralization, regulation of cytoskeletal tissue, standard Wnt

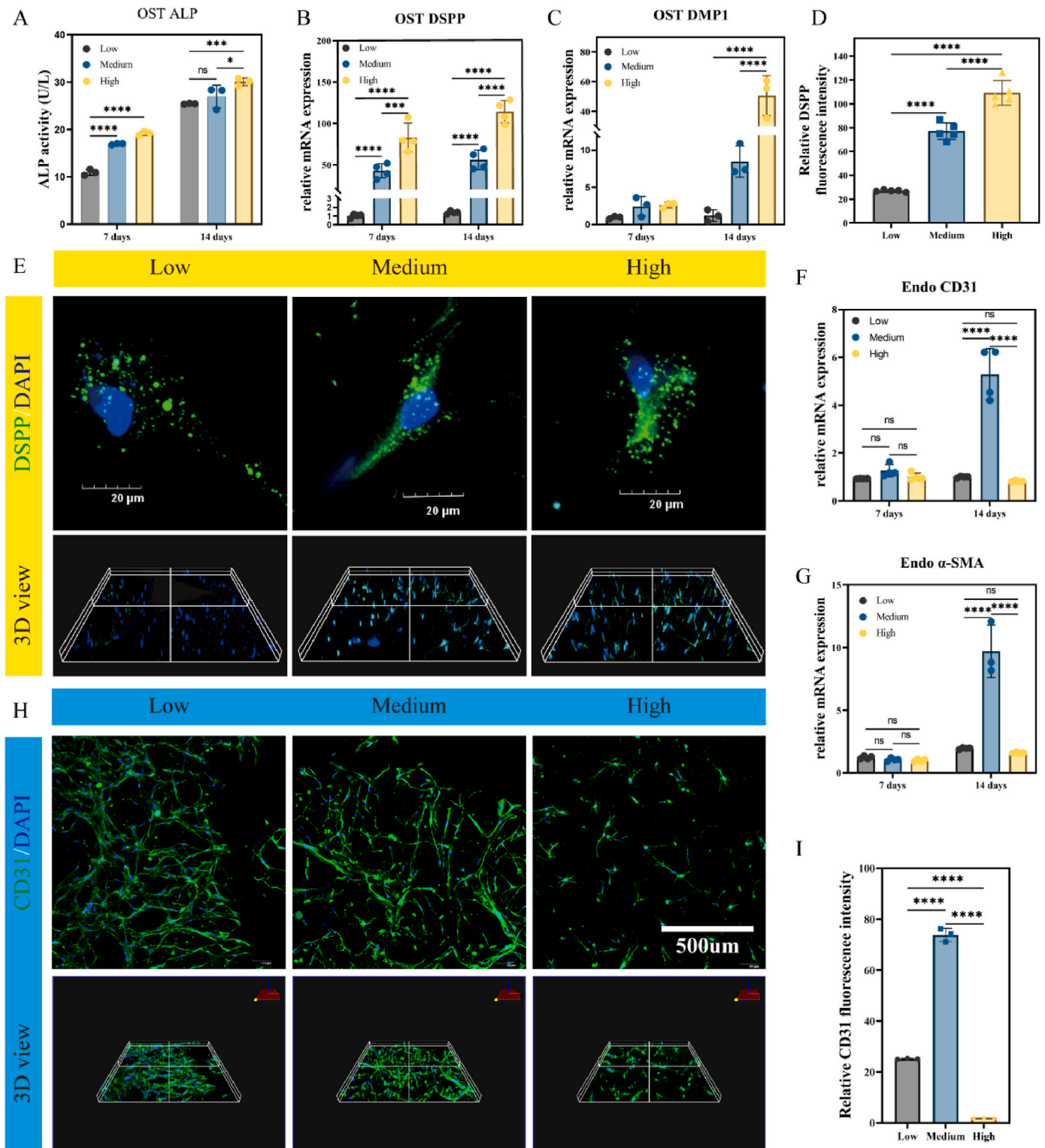


Fig. 3. 3D matrix stiffness synergized lineage specification of HDPSCs. 3D stiffness in combination with osteogenic induction medium in odontogenic differentiation of HDPSCs. A) Alkaline phosphatase activity in HDPSCs cultured with different matrix stiffness gel for 7 and 14 days ($n = 3$). The relative gene expression levels of B) DSPP and C) DMP-1 of HDPSCs ($n = 4$). D-F) Representative images and quantitative analysis of IF staining for DSPP in HDPSCs treated with different stiffness for 14 days. ($n = 3$ randomly-selected microscopic images). Scale bars = 20 μm . 3D stiffness in combination with angiogenesis induction medium in angiogenesis differentiation of HDPSCs. F-G) The relative gene expression levels of CD31 and α -SMA of HDPSCs ($n = 4$). H-I) Representative images and quantitative analysis of IF staining for CD31 in HDPSCs treated with different stiffness for 14 days. ($n = 4$ randomly-selected microscopic images). Scale bars = 100 μm . Results are presented as mean \pm SD. Statistical significance: * $P < 0.05$, ** $P < 0.01$, *** $P < 0.001$, **** $P < 0.0001$. Tukey back testing was used after one-way analysis of variance.

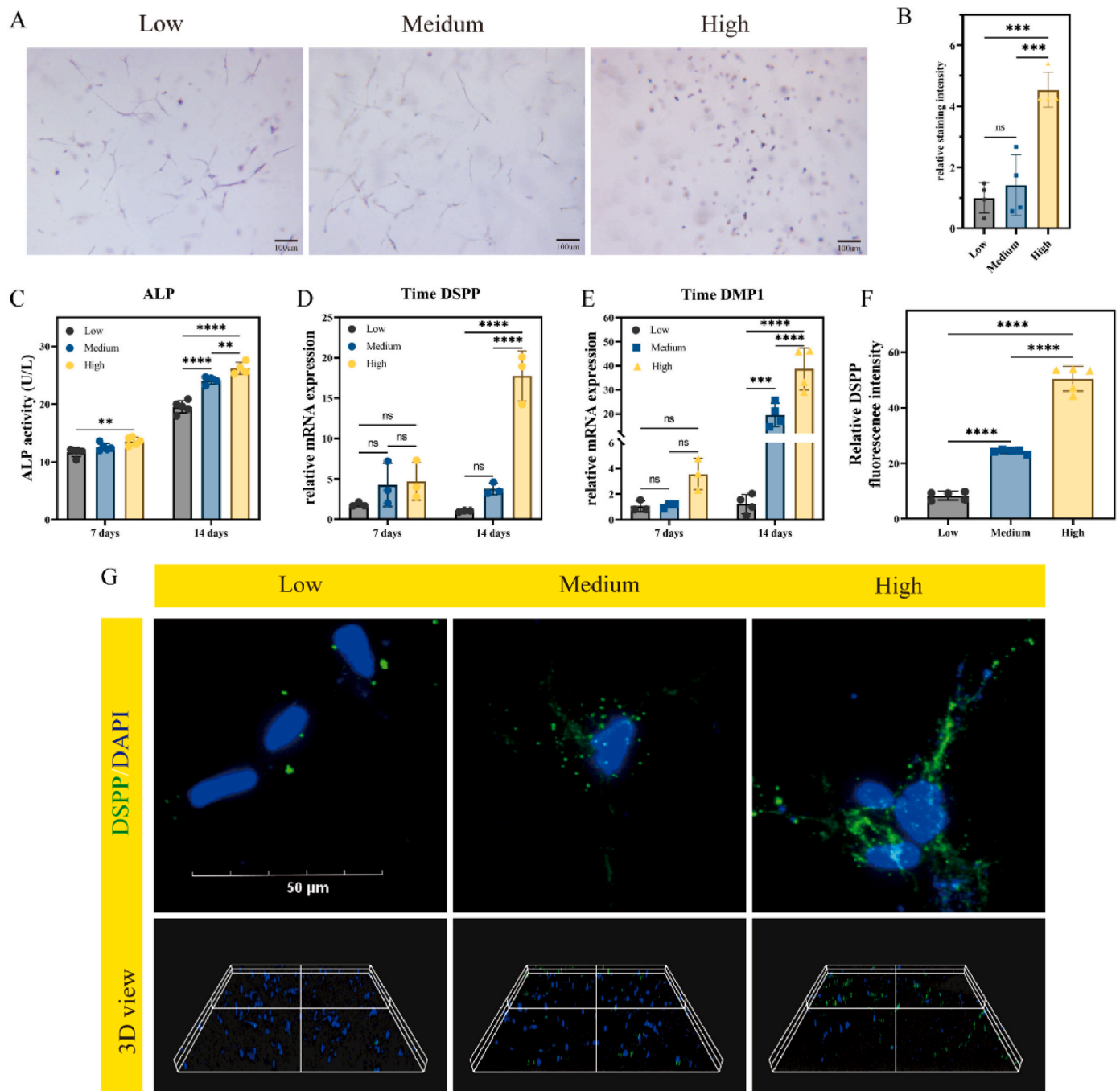


Fig. 4. 3D matrix stiffness directed lineage specification of HDPSCs. A) ALP staining images of HDPSCs embedded in different matrix stiffness at 7 days. B) Semi-quantitative analysis of ALP staining ($n = 4$). C) ALP activity of HDPSCs cultured in gel with different matrix stiffness for 7 and 14 days ($n = 3$). D-E) The relative gene expression levels of DMP-1 and DSPP of HDPSCs ($n = 3$). F-G) Representative images and quantitative analysis of IF staining for DSPP in HDPSCs treated with different stiffness for 14 days. ($n = 4$ randomly selected microscope images). Results are presented as mean \pm SD. Statistical significance: * $P < 0.05$, ** $P < 0.01$, *** $P < 0.001$, **** $P < 0.0001$. Tukey back testing was used after one-way analysis of variance.

signaling pathways, and regeneration were up-regulated in the high stiffness group. Interestingly, BP enrichment results showed the expression of differential genes related to extracellular structure and collagen metabolism, as well as the expression of a large number of genes related to alcohol biosynthetic process suggesting that three-dimensional matrix stiffness might promote the odontogenic differentiation of HDPSCs by affecting lipid metabolism (Fig. S3B). Kurotaki et al. [35] and Ye et al. [36] both proposed the role of lipid metabolism in dentin formation. Gene set enrichment analysis (GSEA) showed that multiple pathways related to cholesterol metabolism were enriched in

the high stiffness group compared to the low stiffness group (Fig. S3C-D and S4). KEGG pathway enrichment analysis revealed the function of DEGs (Fig. 6D). The results showed that the high stiffness may promote the dentin differentiation of HDPSCs through Wnt signaling pathway or FoxO signaling pathway. The role of Wnt pathway in dentin formation has attracted wide attention [37,38], We further explored the role of the Wnt pathway in this process. Differentially enriched genes in the Wnt pathway (Fig. 6E), and the Wnt pathway was explored using protein-protein interactions (Fig. 6F), and the results showed that JUN played an important role as a regulator of osteoblast

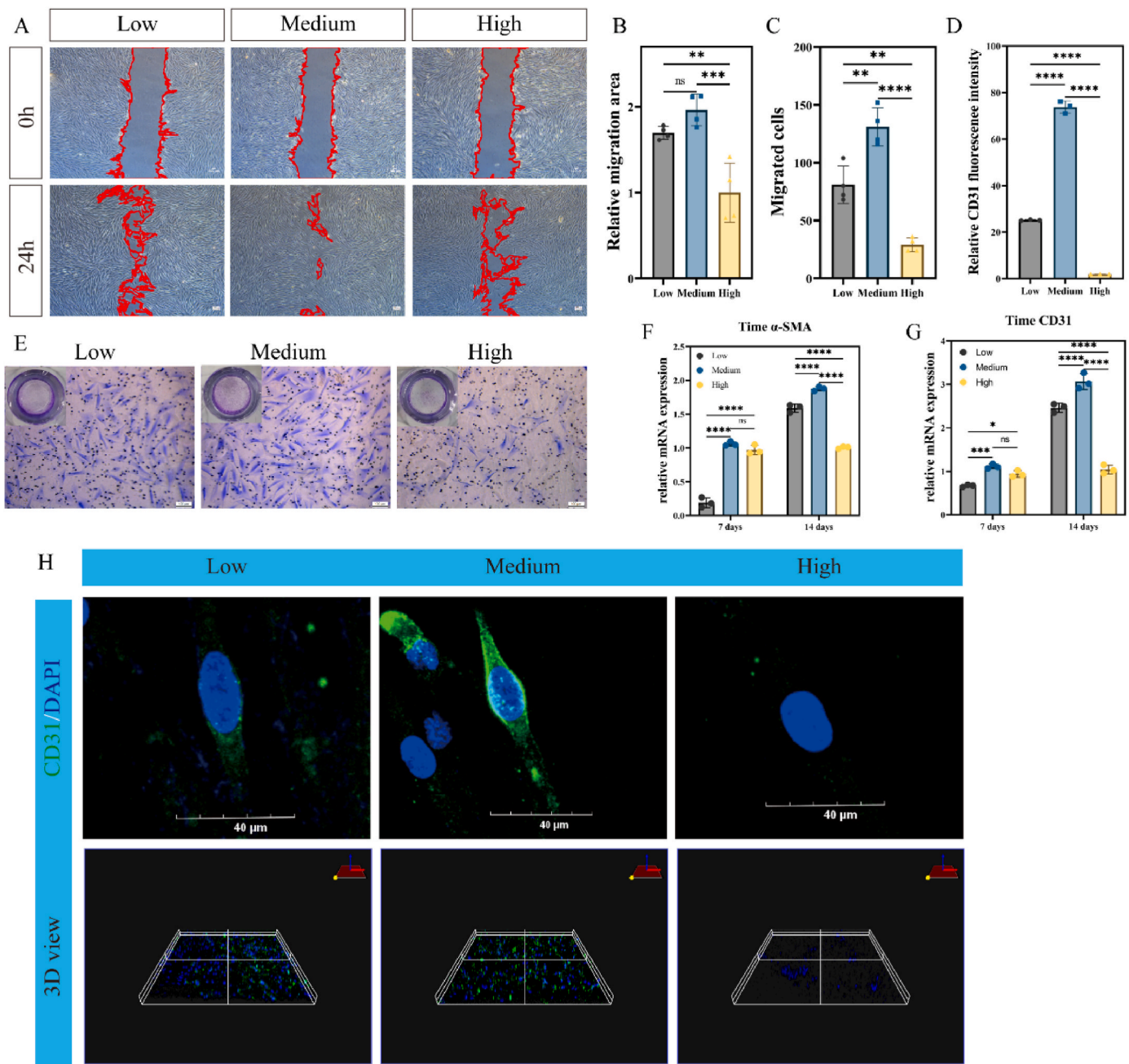


Fig. 5. 3D matrix stiffness directed lineage specification of HDPSCs. A-B) Scratch test image and quantitative analysis of HDPSCs cultured in CMs with different matrix stiffness for 24h (n = 4). C) and E) Transwell image and quantitative analysis of HDPSCs cultured in CMs with different matrix stiffness for 24h (n = 4). F-G) The relative gene expression levels of CD31 and α -SMA of HDPSCs (n = 3). H) and D) Representative images and quantitative analysis of IF staining for CD31 in HDPSCs treated with different stiffness for 14 days. (n = 4 randomly selected microscope images). Results are presented as mean \pm SD. Statistical significance: *P < 0.05, **P < 0.01, ***p < 0.001, ****p < 0.0001. Tukey back testing was used after one-way analysis of variance.

differentiation, which can activate bone homeostasis [39,40]. Therefore, we speculated that matrix stiffness activated lipid/alcohol metabolism through Wnt pathway, thereby activating bone metabolism. The key genes in Wnt pathway were verified by RT-qPCR, and the results showed that Wnt and β -catenin were highly expressed in high stiffness group (Fig. 6G and H). These results indicated that Wnt pathway might play an important role in odontogenesis induced by stiffness. However, it still needs a lot of follow-ups work to verify.

Further, this study explored the protentional mechanism of 3D matrix stiffness promoting vascular differentiation of HDPSCs. Pair-to-pair comparisons showed 2547 unique genes in the medium stiffness group and 2983 unique genes in the high stiffness group (Fig. 7B). Cluster heat

map analysis visualized angiogenesis associated DEGs within each group, with significant differences between the medium and high stiffness groups (Fig. S5A). Compared with the control group, HDPSCs in the medium stiffness group significantly upregulated the expression of genes associated with circulatory process, angiogenesis, germinating angiogenesis, and negative regulation of endothelial cell proliferation (Fig. 7C). BP enrichment results also showed that differential genes related to circulatory system processes, regulation of vasoconstriction, blood circulation, and positive regulation of blood circulation were significantly enriched (Fig. S5B). In addition, KEGG pathway enrichment analysis revealed the function of DEGs (Fig. 7D). The analysis results indicated that the medium stiffness group may promote vascular

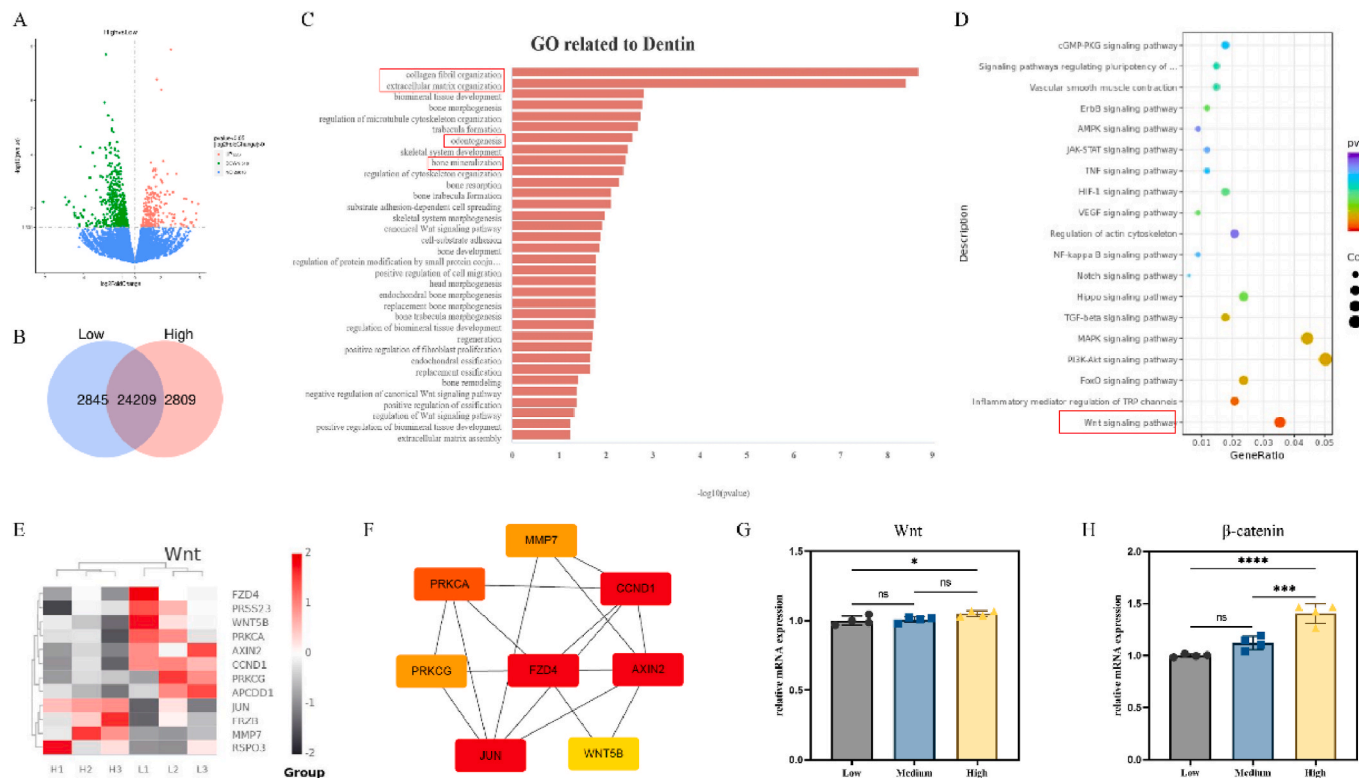


Fig. 6. RNA-seq revealed extensive transcriptomic changes of HDPSCs induced by three-dimensional matrix stiffness. A) Volcano maps of gene expression levels between High and Low groups. B) Co-express Venn diagram of Low group and High group. C) REVIGO analysis clustering all GO terms of BP into a broader category (High vs Low). D) KEGG analysis of differential genes in HDPSCs (High vs Low). E) Heatmap of Wnt signaling pathway. F) Protein-protein interaction network of Wnt signaling pathway related genes. G-H) The relative gene expression levels of Wnt and β -catenin of HDPSCs ($n = 4$). Results are presented as mean \pm SD. Statistical significance: * $P < 0.05$, ** $P < 0.01$, *** $p < 0.001$, **** $p < 0.0001$. Tukey back testing was used after one-way analysis of variance.

differentiation of HDPSCs by up-regulating PI3K-Akt signaling pathway, MAPK signaling pathway, TGF-beta signaling pathway and other pathways. The GSEA diagram also showed that compared with the control group, the three-dimensional matrix stiffness in the medium stiffness group might play a role by activating the PI3K-Akt signaling pathway and TGF-beta signaling pathway (Fig. S5C). We further explored the role of the PI3K-Akt pathway in this process. Differentially enriched genes in the PI3K-Akt pathway (Fig. 7E), and the PI3K-Akt pathway was explored using protein-protein interactions (Fig. 7F), and the results showed that PDGFA played an important role. PDGFA has the function of promoting angiogenesis [41]. The key genes in PI3K-Akt pathway were verified by RT-qPCR, and the results showed that PI3K and Akt were highly expressed in medium stiffness group (Fig. 7G and H). These results indicated that PI3K-Akt pathway might play an important role in vascular differentiation induced by matrix stiffness.

3.5. Paracrine signals of HDPSCs triggered by stiffness regulate periapical resident cell behaviors

In the field of tissue engineering and regenerative medicine, the paracrine function of stem cells, that was, their ability to secrete bioactive molecules, was increasingly becoming the focus of research [42,43]. These bioactive molecules, including cytokines, growth factors, enzymes, as well as ECM components, played a vital role in tissue repair and regeneration through paracrine signaling [44]. The aim of this study was to evaluate how 3D matrix stiffness affected the fate of periapical cells by regulating paracrine signaling of HDPSCs.

Using RNA sequencing, we identified the expression levels of genes encoding secreted proteins. A list of genes encoding secreted proteins was obtained from the Human Protein Atlas database. In this sequencing project, we matched 3865 genes encoding secreted proteins. A cluster

heat map analysis was performed on the parts of these genes with significant expression differences. And the results showed that three-dimensional matrix stiffness significantly affected the secreted proteome genes of HDPSCs (Fig. 8A). Further GO analysis revealed the functions of these DEGs at three levels: BP, CC and MF. Particularly among the top 10 biological processes, we observed significant differences related to proteins, tissue humoral immune responses, and extracellular matrix (Fig. 8B). These factors were involved in various biological processes that regulated tissue repair and regeneration, including positive regulation of endothelial cells, extracellular structure organization, extracellular matrix organization, collagen metabolic processes, defense responses to other organism, humoral immune responses, etc. (Fig. 8C).

In summary, three-dimensional matrix stiffness might play an important role in the proliferation and differentiation of periapical resident cells, including endothelial cells, immune cells, and fibroblasts, through paracrine signaling. In order to further investigate this phenomenon, we studied the effects of paracrine factors of HDPSCs cultured under different three-dimensional matrix stiffness conditions on the cell behavior of periapical resident cells. To this end, we collected CM of HDPSCs cultured under low, medium, and high stiffness conditions and applied them to HUVECs, THP-1 macrophages and HSF cultures to assess the effects of these presecretory factors on cell behavior.

3.5.1. Paracrine signals of HDPSCs triggered by stiffness regulate HUVECs behaviors

Angiogenesis was a key activity during tissue healing, because it provided blood vessels that provides oxygen and nutrients to cells in damaged tissue [45]. The premise of pulp regeneration was that there are vessels, but the root tip was narrow, preventing the growth of vessels [46]. It had been shown that dental stem cells were not only directly

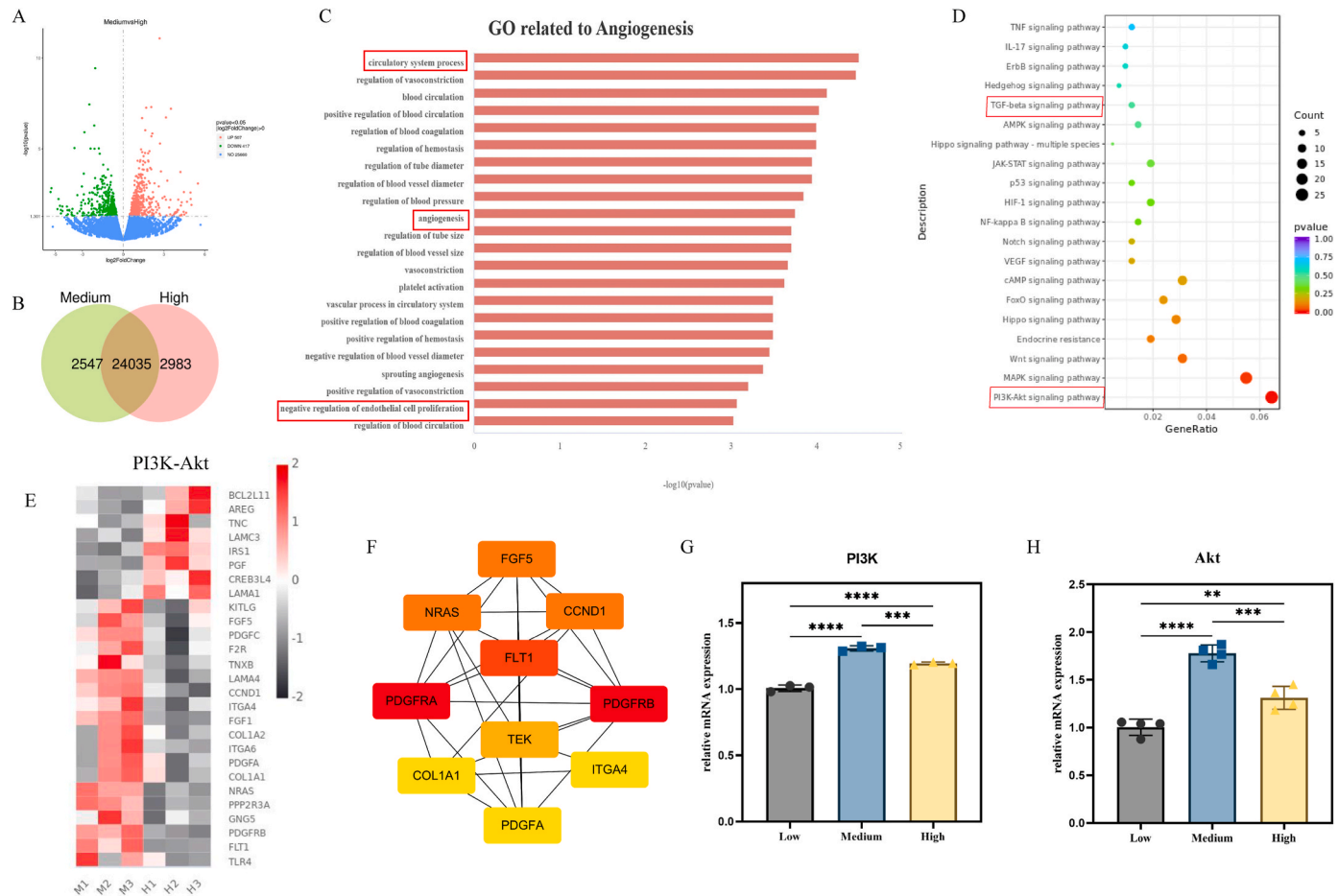


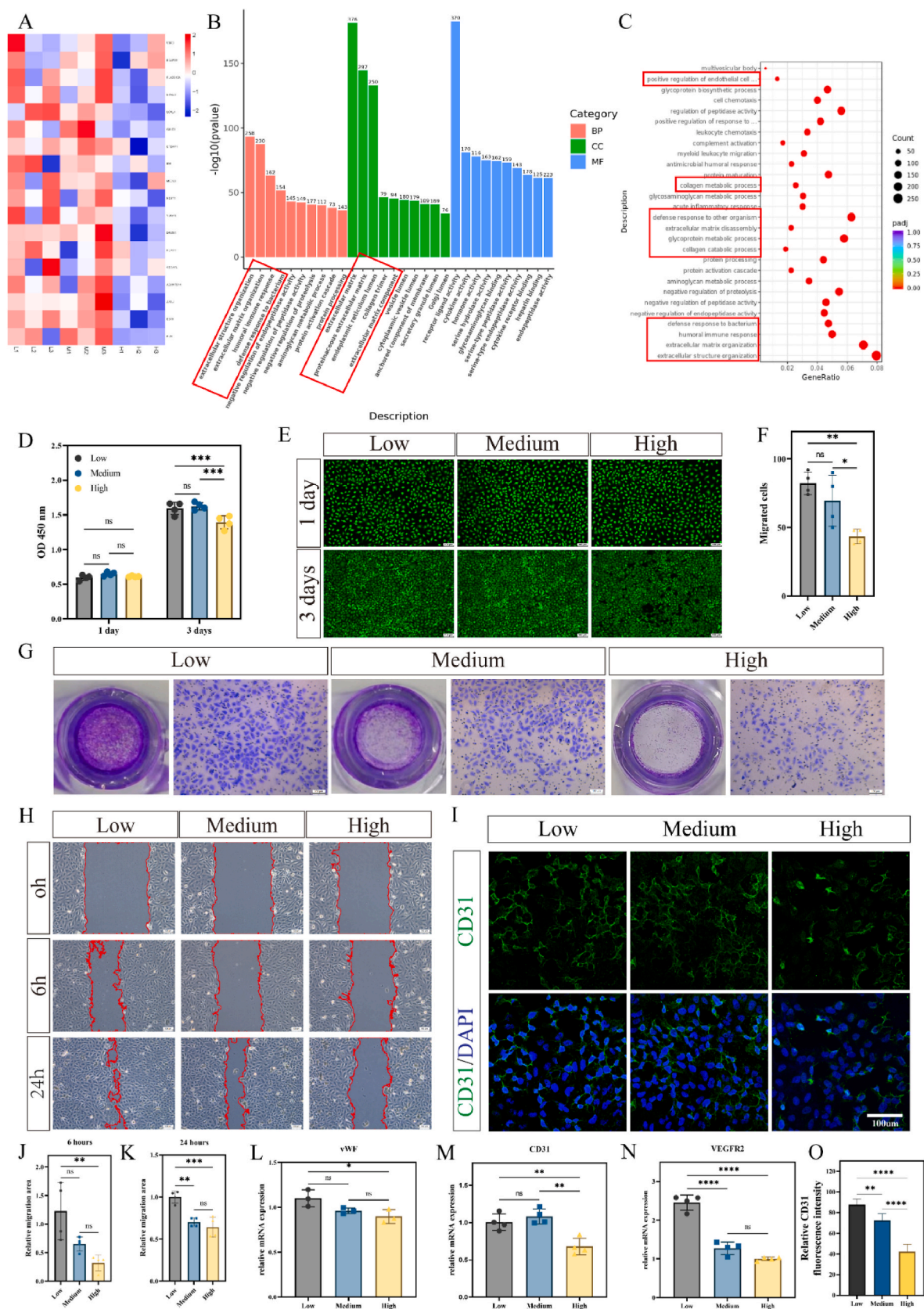
Fig. 7. RNA-seq revealed extensive transcriptomic changes of HDPSCs induced by three-dimensional matrix stiffness. A) Volcano maps of gene expression levels in Medium and High groups. B) Co-express Venn diagram of Medium and High group. C) REVIGO analysis clustering all GO terms of BP into a broader category (Medium VS High). D) KEGG analysis of differential genes in HDPSCs (Medium VS High). E) Heat map of PI3K-Akt signaling pathway. F) Protein–protein interaction network of PI3K-Akt signaling pathway related genes. G–H) The relative gene expression levels of PI3K and Akt of HDPSCs (n = 4). Results are presented as mean \pm SD. Statistical significance: *P < 0.05, **P < 0.01, ***p < 0.001, ****p < 0.0001. Tukey back testing was used after one-way analysis of variance.

involved in angiogenesis through differentiation into endothelial cells, but also stimulate angiogenesis through paracrine angiogenesis factors [47]. We hypothesized that paracrine factors of HDPSCs embedded in three-dimensional matrix stiffness could promote periapical vascular growth. CCK-8 showed that the cell proliferation of HUVECs was significantly increased after 3 days of treatment with HDPSCs paracrine factor. And the HUVECs proliferation in the low stiffness and medium stiffness groups was significantly higher than that in the high stiffness ($P < 0.001$) (Fig. 8D). After 1 and 3 days of culture, the viability of cells in each group were confirmed by live staining, which was consistent with the trend of CCK-8 (Fig. 8E). In order to evaluate the effect of paracrine factors on the HUVECs migration, transwell assay was performed. transwell chamber was used to evaluate the attractiveness of paracrine factors of HDPSCs to cells in different matrix stiffness. We counted the number of cells that migrated to the transwell membrane. The number of cell stiffness in the low stiffness (82.25 ± 7.15) and medium stiffness (69.50 ± 16.14) was significantly more than that in the high stiffness (43.50 ± 4.60) ($P < 0.05$) (Fig. 8F and G). After verifying that low stiffness and medium stiffness were more acceptable to HUVECs cells, we performed scar test to verify the migration and repair ability of paracrine factors. HUVECs migration was assessed at 6 and 24 h. The result and statistics of cell stiffness are shown in Fig. 8H and K. In general, the cells in the low stiffness CM were the fastest. After 6 h, low stiffness was significantly higher than high stiffness ($P < 0.01$), and the trend remained the same 24 h later. RT-qPCR was used to detect the expression of vascular markers, including vWF, CD31 and VEGFR2. As

shown in Fig. 8L–N, all angiogenesis genes increased significantly in the low stiffness. After 3 days of culture of HUVECs with paracrine factors, the expression of vascular markers in cells was tested. The protein expression of CD31 was detected, as shown in Fig. 8I and O, the expression of HUVECs in the low stiffness group was significantly higher than that in the medium and high stiffness groups ($P < 0.001$). The results were consistent with the trend of RT-qPCR. In conclusion, paracrine factors in the low stiffness group were the best for the vascular stiffness of HUVECs.

3.5.2. Paracrine signals of HDPSCs triggered by stiffness regulate THP-1 macrophages behaviors

In periapical inflammatory, macrophages have been shown to be the major immune active cells [48]. Inflammation was an early response mediated by various immune cells during apical healing to eliminate cellular debris, foreign bodies, and bacteria [49]. Macrophages were one of the first immune cell types to arrive at the inflammation and mediate an acute proinflammatory response for several days. Subsequently, the proinflammatory (M1) macrophage phenotype switched to an anti-inflammatory (M2) phenotype, which could promote inflammation resolution, tissue remodeling, and neovascularization, thereby accelerating tissue healing [50]. However, malfunction of macrophage phenotype switching could lead to chronic inflammation in some diseases, such as diabetes, thereby inhibiting tissue healing [45]. Due to the immunomodulatory effects of 3D matrix stiffness on HDPSCs, we investigated the effects of their paracrine products on macrophage



(caption on next page)

Fig. 8. 3D matrix stiffness stimulated paracrine signals of HDPSCs in vitro to regulate angiogenesis in HUVECs. A) Heat map of cluster analysis. B) GO analysis to analyze the function of DEG at three levels: biological process (BP), cell component (CC), and molecular function (MF). C) REVIGO analysis clustered all GO terms of BP into broader categories. D) The proliferation of HUVECs treated with different CMs for 1 and 3 days was measured by CCK-8 ($n = 4$). E) The cell viability of HUVECs treated with different CMs for 1 and 3 days was observed by Live/Dead staining. F-G) Representative images and quantitative analysis of transwell for HUVECs after 24h treatment by different CMs ($n = 4$). H) The representative images of HUVECs migration at 0, 6 and 24h under different CMs treatment were observed by scratch assay. I) Scratch assay to observe HUVECs migration at 6h under different CMs treatments ($n = 4$). J) Scratch assay to observe HUVECs migration at 24h under different CMs treatments ($n = 4$). K) Representative images of IF staining for CD31 of HUVECs treated with different CMs for 3 days. Scale = 100 μm . L) Quantitative results of IF staining for CD31 of HUVECs treated with different CMs for 3 days ($n = 4$ randomly selected microscope images). M-N) The relative gene expression levels of vWF, CD31 and VEGFR2 in HUVECs treated with different CMs for 3 days ($n = 4$). The data were expressed as mean \pm SD. Statistical significance: * $P < 0.05$, ** $P < 0.01$, *** $P < 0.001$, **** $P < 0.0001$. Tukey back testing was used after one-way analysis of variance.

polarization by IF staining and RT-qPCR. Macrophages were identified by detecting the macrophage surface marker CD11b by flow cytometry. The results showed that PMA successfully induced THP-1 monocytes into THP-1 macrophages (Fig. 9A and B). Differential receptor expression was the key feature of polarized macrophages [51]. Laser confocal microscopy was performed to image the polarization expression markers of THP-1 macrophages. The M1 phenotype was characterized by increased expression of CD86, while M2 phenotype usually expressed CD206. As shown in Fig. 9C and D, the expression of CD86 in THP-1 macrophages (considered to be M0 phenotype) treated with paracrine factors in the low stiffness group was significantly lower than other groups ($P < 0.0001$), and the expression of CD206 was significantly higher than that in the medium and high stiffness group ($P < 0.0001$), indicating that the paracrine factors in the low stiffness could induce M0 macrophages to M2 phenotype. After verifying the cell phenotypic proteins, we performed RT-qPCR on all groups, mainly detecting the mRNA that could secrete pro-inflammatory specific antibodies (iNOS, IL-6) and anti-inflammatory specific antibodies (Arg-1, IL-4). The results showed that the CM by low stiffness matrix induced THP-1 macrophages to secrete more anti-inflammatory cytokines and showed better immunoregulation (Fig. 9G and H). On the contrary, the secretion of pro-inflammatory cytokines in THP-1 macrophages induced by CM with high stiffness matrix was significantly higher (Fig. 9E and F). Overall, HDPSCs in low stiffness matrix induced higher levels of anti-inflammatory macrophages.

3.5.3. Paracrine signals of HDPSCs triggered by stiffness regulate HSF behaviors

Fibroblasts were mesenchymal cells with multiple functions, including ECM deposition, regulation of epithelial differentiation and immune regulation, and were involved in tissue remodeling and healing [52]. At the end of the inflammatory phase, fibroblasts migrated to the damaged area, proliferates, mediates fibrin clot degradation and ECM deposition, and ultimately initiates the proliferation phase of tissue healing [53]. In order to evaluate the potential of paracrine signaling of HDPSCs in tissue repair under the influence of 3D matrix stiffness, we studied their effects on HSF behavior. CCK-8 assay showed that paracrine factors could promote the proliferation of HSF Indiscriminately (Fig. 9I). In addition, we only used live staining solution to detect cell viability. The results showed that HSF in each group showed bright green, evenly distributed and stretched in shape (Fig. 9J). Subsequently, we evaluated the effects of different CMs on HSF migration using scratch assay. Representative images and quantitative analysis showed that compared with paracrine factors in the high stiffness group, paracrine signals induced by low stiffness significantly promoted the migration of fibroblasts (Fig. 9L and M). VEGF was a highly specific pro-vascular endothelial cell growth factor that promoted increased vascular permeability, extracellular matrix degeneration, vascular endothelial cell migration, proliferation and blood vessel formation. The expression of VEGF-A increased during the proliferation phase of healing [54]. We detected the protein expression of VEGF in HSF. As shown in Fig. 9K and N, the paracrine signaling induced by low stiffness significantly promoted the protein expression of VEGF ($P < 0.001$), indicating that the paracrine signaling of HDPSCs induced by low stiffness could enhance the angiogenic potential of HSF. In short, these findings indicated that

paracrine factors of HDPSCs induced by low stiffness matrix could promote fibroblast proliferation, viability, and migration. Among them, paracrine signaling stimulated by low stiffness could enhance the angiogenic potential of fibroblasts, which is beneficial to the periapical tissue healing and regeneration.

In summary, we found an interesting conclusion that pulpodentinal complex regeneration could not be supported by a single stiffness alone, but required the synergistic effect of different stiffnesses, which was consistent with the view of Yu et al. [31]. High stiffness (about 24.12 kPa) was conducive to inducing HDPSCs to differentiate into odontoblasts and promoted hard tissue regeneration; medium stiffness (about 6.37 kPa), close to the stiffness of physiological pulp, was conducive to inducing HDPSCs to differentiate into endothelial cells and promote angiogenesis; low stiffness (about 0.79 kPa) was conducive to inducing the paracrine signaling of HDPSCs to promote periapical tissue regeneration, including promoting the angiogenic ability of HUVECs, promoting the transformation of THP-1 macrophages to anti-inflammatory direction, and promoting the proliferation, vitality, migration and angiogenic potential of HSF. Combining the advantages of three-dimensional matrix stiffness, we proposed "Tri-Phase Biomechanical Structure" to promote pulp regeneration (Fig. 10C). The crown was the high stiffness matrix to induce crown sealing; the middle of the root canal was the medium stiffness matrix to promote pulp tissue regeneration that matched the physiological pulp; the apical was the low stiffness matrix to promote the ingrown of periapical tissue through the paracrine effect of HDPSCs.

3.6. Tri-phase biomechanical structure promoted complete pulpodentinal complex regeneration in vivo

Modeling process. In order to verify that Tri-Phase Biomechanical Structure hydrogel could be effectively used for potential dental pulp regeneration in vivo, we used a nude mouse subcutaneous transplantation model (Fig. 10A). In this study, BALB/c nude mice were selected as an in vivo model to avoid immune rejection of the transplant. To simulate the root environment, the root was shaped into a cylindrical shape with a height of about 5–8 mm, and then treated with a series of chemical reagents to prepare TDM. The sterilized TDM was placed in complete culture medium and incubated overnight. The culture medium was observed to be clear and sterile under a microscope. HDPSCs were pre-seeded in three hydrogels with low, medium and high stiffness, and then materials were injected into the TDM in different ways according to the different structures (Fig. 10C). The first group was "Blank", which was TDM without injection of any material. The second group was "Medium", that HDPSCs were embedded in the medium stiffness hydrogel and injected into the TDM. The third group was "Tripartite". The Tri-Phase structure was tripartite in TDM. HDPSCs was pre-embedded in hydrogels of three stiffnesses, and then low stiffness hydrogels were injected into the root apex, medium stiffness hydrogels were injected into the middle of the root canal, and high stiffness hydrogels were injected into the crown of the root canal. Subsequently, they were immediately implanted subcutaneously in immunodeficient mice (Fig. S6). The wound healed well after surgery, and the appearance of the healed skin was close to normal. (Fig. 10B). Eight weeks after surgery, new tissue-like structures were observed in all implanted TDMs,

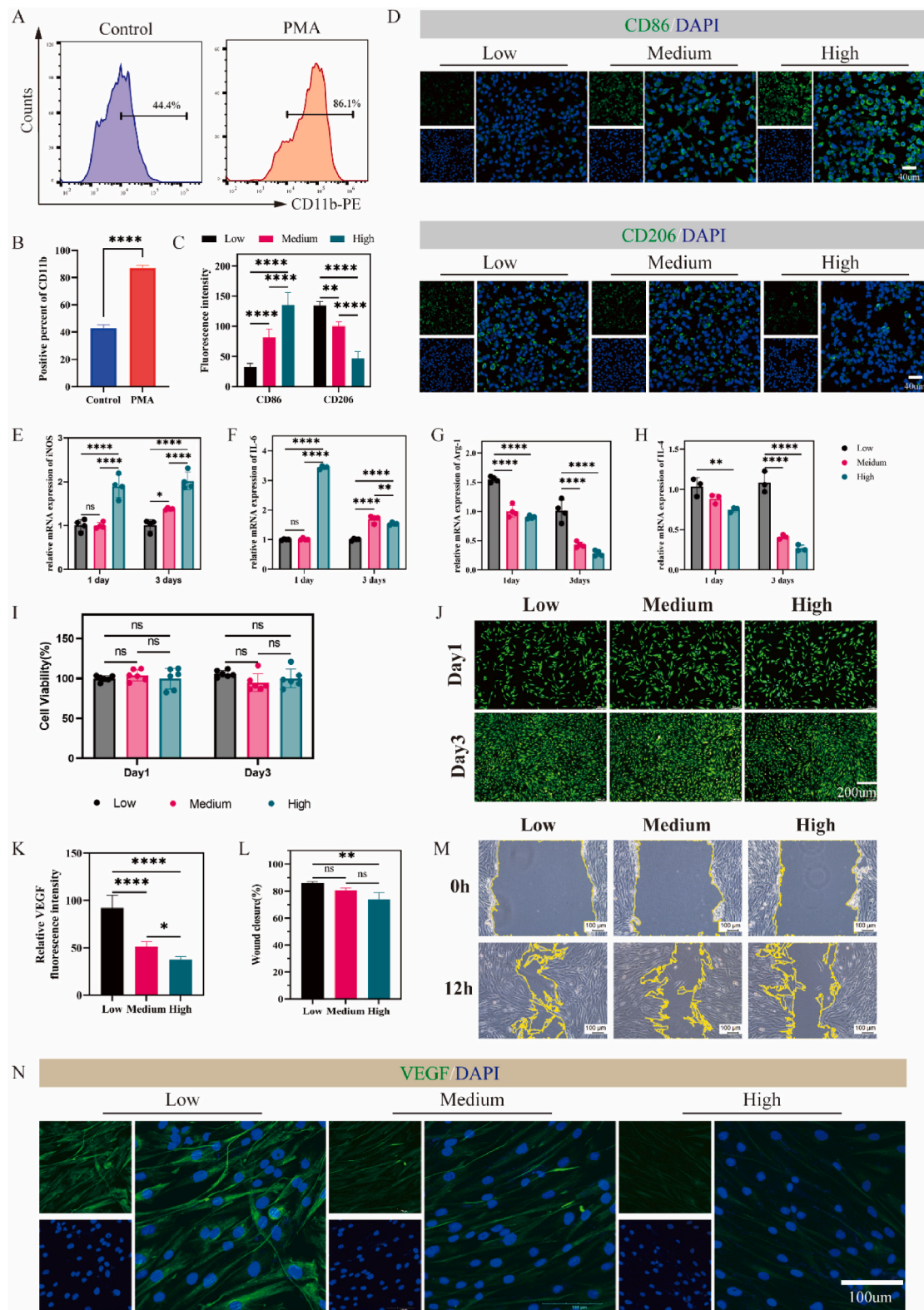


Fig. 9. 3D matrix stiffness stimulated paracrine signals of HDPPSCs in vitro to regulate cell behavior of THP-1 macrophages and HSF. A-B) The expression of CD11b on THP-1 cells differed significantly between the control and PMA group (biological repeats). C-D) Representative images and quantitative analysis of CD86 and CD206 IF staining of macrophages treated with different CMs for 3 days ($n = 3$ randomly selected microscope images). E-H) The relative gene expression levels of iNOS, IL-6, Arg-1 and IL-4 in THP-1 macrophages treated with different CMs at 1 and 3 days ($n = 4$). I) Proliferation of HSF cells treated with different CM for 1 and 3 days was determined by CCK-8 ($n = 6$). J) The cell viability of HSF treated with different CMs at 1 and 3 days was observed by Live/Dead staining. L-M) Representative images and quantitative analysis of cell migration of HSF cells treated with different CMs at 0 and 12 h were observed by scratch assay ($n = 3$ randomly selected microscope images). K and N) Representative images and quantitative analysis of IF staining for VEGF under different CMs treatment for 3 days ($n = 6$ randomly selected microscope images). The data were expressed as mean \pm SD. Statistical significance: * $P < 0.05$, ** $P < 0.01$, *** $p < 0.001$, **** $p < 0.0001$. Tukey back testing was used after one-way analysis of variance.

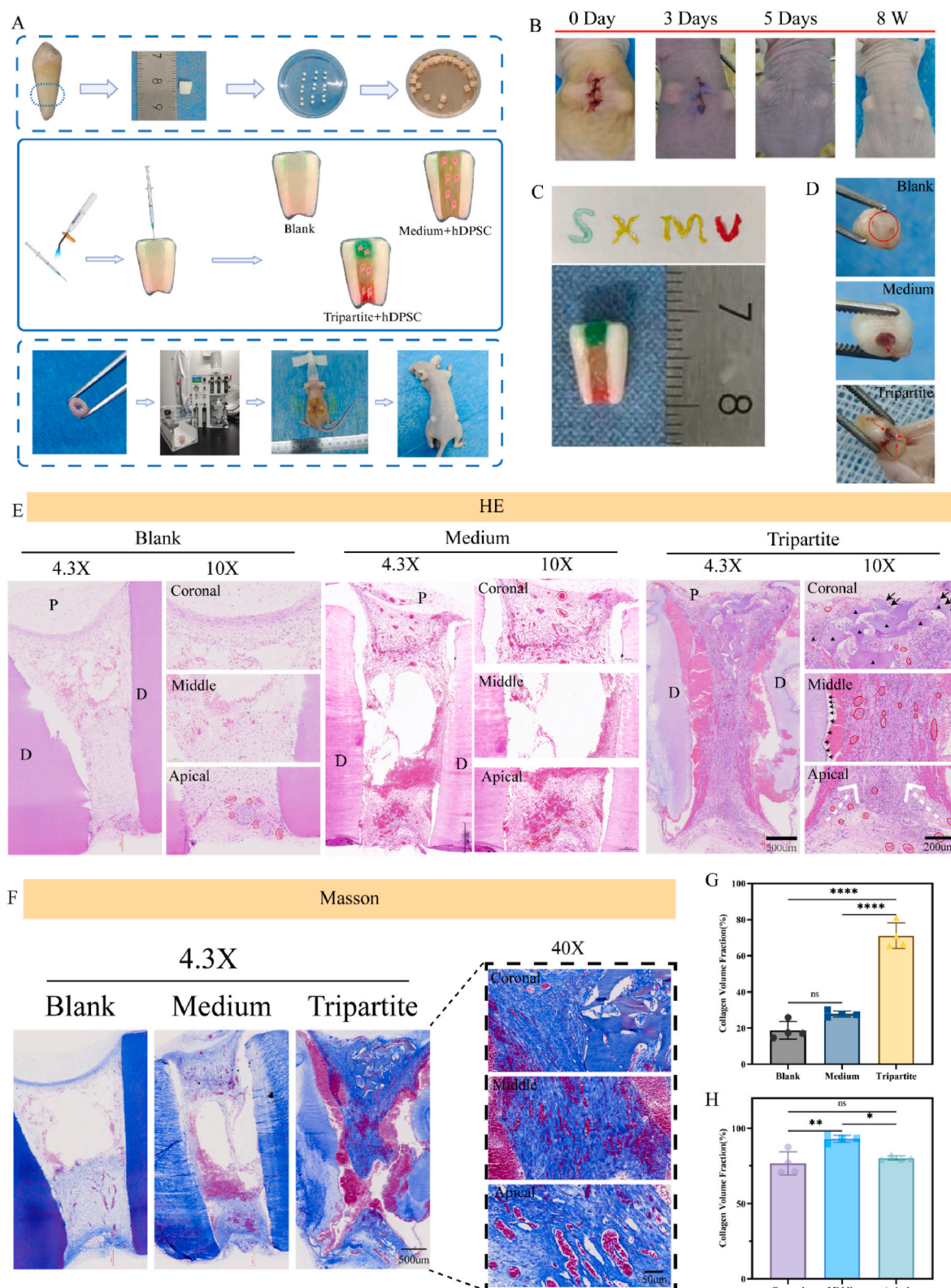


Fig. 10. Tri-Phase Biomechanical Structure promoted regeneration of dentinopulp complex in vivo. A) TDM implanted with Tri-Phase Biomechanical Structure hydrogel under the skin of the BALB/c nude mice. The Tri-Phase structure with hDPSCs was tripartite in TDM. The crown of the root canal was high stiffness hydrogel, the middle part of the root canal was medium stiffness hydrogel, and the root apex was low stiffness hydrogel. B) Wound healing at different time points. C) Injectable Models. D) Representative images after 8 weeks of subcutaneous transplanted TDM in the Blank, Medium, and Tripartite groups. E) HE staining images at 8 weeks. F) Representative micrographs of regenerated medullary tissue in TDM of Blank, Medium and Tripartite groups after Masson tricolor staining, with scale bars of 500 μ m and 200 μ m. G-H) Semi-quantitative analysis of collagen volume fraction in pulp-like tissue. The data were expressed as mean \pm SD. Statistical significance: * $P < 0.05$, ** $P < 0.01$, *** $P < 0.001$, **** $P < 0.0001$. Tukey back testing was used after one-way analysis of variance.

even in the control group (Fig. 10D). The blood vessels grew around the root apex in the Medium and Tripartite groups, and the tripartite group had significantly richer vascular tissue ingrown.

Biosafety assessment. Although the excellent biocompatibility of GelMA hydrogels with different physiological dynamics had been verified in vitro, safety needed to be established in vivo to assess its non-toxic effects on animals. Therefore, HE staining was performed on different visceral sections at 8 weeks. HE staining showed that there were no significant differences in various organs among groups, which proved that the hydrogel had no obvious toxicity to nude mice (Fig. S7A). Secondly, hydrogel extracts with different matrix stiffness were mixed with blood cells of nude mice to determine their hemolysis. Under natural light, there was no obvious hemolysis phenomenon in the EP tubes of all hydrogels. The hemolysis rate was calculated by testing the absorbance at 545 nm, and the results showed the hemolysis rate of all hydrogel stiffness groups was extremely low (less than 5 %) (Fig. S7B). In summary, it was proved that gelatin hydrogels with different stiffness had good biocompatibility in nude mice, which could be used for subsequent in vivo application research.

HE staining. As shown in Fig. 10E, all groups were filled with new tissues. But compared with Tripartite group, Blank group and Medium group was obviously empty in the middle part of the root canal, while nearly no tissues were observed. The Blank group had obvious vacuolar structure in the root canal with a large amount of adipose tissue, and only a small amount of blood vessels was found (shown by red circles in Fig. 10E). The dental pulp-like tissues in the Medium group were distributed at both ends of the root canal and was composed of blood vessels and fibers. Dental pulp-like tissues in the Tripartite group filled the whole root canal, and a large number of new mineralized tissues were formed in the crown side (shown by black triangle in Fig. 10E), surrounded by neat odontoblast-like cells (shown by black arrow in Fig. 10E). The mineralized area was about 0.9 mm², accounting for about 32 % of the cavity area of the crown side. This was due to the induction of HDPSCs in high stiffness. There were a large number of fibrous tissues and blood vessels in the middle of the root canal. On the interface between the regenerated soft tissue and the dentin, linear cells were concentrated in the inner edge of the dentin. And protrusion could be seen penetrating into the dentin tubules (shown by the black arrow in Fig. 10E). Abundant fibers (indicated by white arrows in Fig. 10E) and blood vessels were seen in the apex of the root from the outer perimeter and fused with the new pulp-like tissue. This might be due to paracrine effects of HDPSCs induced by low stiffness. The above results were consistent with the trend of cell experiment.

Masson staining. As collagen fibers were the most important dental pulp matrix, it was important to evaluate the formation of collagen fibers to evaluate the maturity of pulp tissue [55]. In Masson staining, light green or aniline blue had a larger molecular weight, so after staining, the muscle fibers appeared red, while the collagen fibers appeared green or blue. At low magnification, more connective tissue and fiber healing were observed in the Tripartite group than in the Blank and Medium groups, suggesting that hydrogels with multiple stiffness synergies were more conducive to the formation of defective soft tissues and collagen fibers (Fig. 10F and G). Further, we analyzed the fiber formation of the new pulp tissue in different regions of the Tripartite group. The results showed that a large number of collagen fibers were formed in all regions, and collagen fibers accounted for more than 70 % of the new tissues (Fig. 7F and H), among which the collagen fibers in the middle of the root canal were significantly higher than those at both ends of the root canal.

Immunohistochemistry. The expression level of DSPP was closely related to the differentiation of odontoblast cells and was a key matrix protein secreted by odontoblast cells. And it was essential for dentin mineralization [56]. Therefore, we performed immunohistochemical staining of DSPP protein in sections. The results showed that DSPP positive staining was found all around the dentin wall (Fig. 11A), and the expression level of DSPP staining in Tripartite group was

significantly higher than that in Medium group (Fig. 11B). Further analysis of DSPP staining in different areas of the Tripartite group showed that deep staining of DSPP protein appeared in the cells around the newly mineralized tissue of the crown part. And it was significantly higher than that in the middle of the root canal and the tip of the root (Fig. 11C), indicating that high stiffness was significantly promoted the mineralization of HDPSCs. At the same time, immunohistochemical staining of CD31 protein was performed (Fig. 11F), and the results showed that there were significantly more vessels in the Tripartite group, followed by the medium group (Fig. 11D). In the Tripartite group, vascular in the middle and apex of the root canal was significantly greater than that in the crown (Fig. 11E). Combined with the empty in the middle of the Medium group, we guessed that most blood vessels in the middle of the root canal were derived from HDPSCs, that was, medium stiffness significantly promoted the angiogenesis of HDPSCs. At the same time, the apical blood vessels grew in from the surrounding tissues and merged with the pulp tissue in the middle of the root canal (Figs. 7F and 8A), indicating that the paracrine factor of HDPSCs in low stiffness was significant.

4. Discussion

In this study, we investigated the effects of matrix stiffness on the differentiation and paracrine functions of HDPSCs in vitro. Additionally, we successfully developed a hydrogel with a “Tri-Phase Biomechanical Structure” for the regeneration of the pulpodentin complex in vivo, aiming to fully leverage the role of the three-dimensional mechanical environment. The Tri-Phase Biomechanical Structure was inspired by physiological tooth structure, comprising a hard crown tissue, a soft pulp tissue in the middle of root canal and vascular fiber tissue in the apical part connected periapical tissue. When bacteria invaded, the hard tissue of the crown is initially compromised, collapsing under the acidic secretions of bacteria. Following the destruction of dentin, bacteria infiltrate the soft pulp tissue and eventually compromise the periapical tissue via blood vessels and other channels [57,58]. Therefore, in the process of repair, we used the “Tri-Phase Biomechanical Structure” hydrogel to restore the structures damaged by bacteria one by one.

Several scholars have tried to achieve complex regeneration of both soft and hard tissue through different structural approaches. Jin et al. employed the sandwich structure composed of HDPSCs sheet/treated dentin matrix (TDM)/Matrigel interlayer for root regeneration [59]. The results showed that TDM promoted the regeneration of soft tissue, such as periodontal connective tissue, and hard tissue, such as dentin at the same time. Additionally, Matrigel promoted the regeneration of soft tissues such as dental pulp cell-like cells and vascular structures in pulp cavity. Similarly, Tian et al. used sandwich structure composite materials (gelatin electrospun tablets (APES)/TDM/DPEM) to promote the regeneration of periodontal tissue and pulp [60]. By simulating the extracellular matrix microenvironment of stem cells, APES had directional fiber orientation, which could guide cell proliferation. Meanwhile, DPEM retained the original fiber structure and ECM protein, both of which promoted the odontogenic differentiation of dental stem cells. Soft tissues such as blood vessels were also generated on the inside of TDM, and periodontal ligament-like soft tissues were generated on the outside of TDM. Bertassonic et al. used pre-vascularized structure for the pulp-like tissue structure of full teeth, and used sacrificial fibers to reserve endothelial colonies in the middle of root canals to form microchannels of cells. The periphery was filled with GelMA hydrogel, forming a concentric structure, which simply and effectively promoted the immediate vascularized pulp regeneration [61]. All above studies showed that complex pulp regeneration needed to provide suitable microenvironment for different components to promote the complex regeneration. On the basis of this view, the Tri-Phase Biomechanical Structure proposed in this study was a further study of above research. This structure was simple, and it was a more suitable clinical method to realize the regeneration of pulpodentin complex.

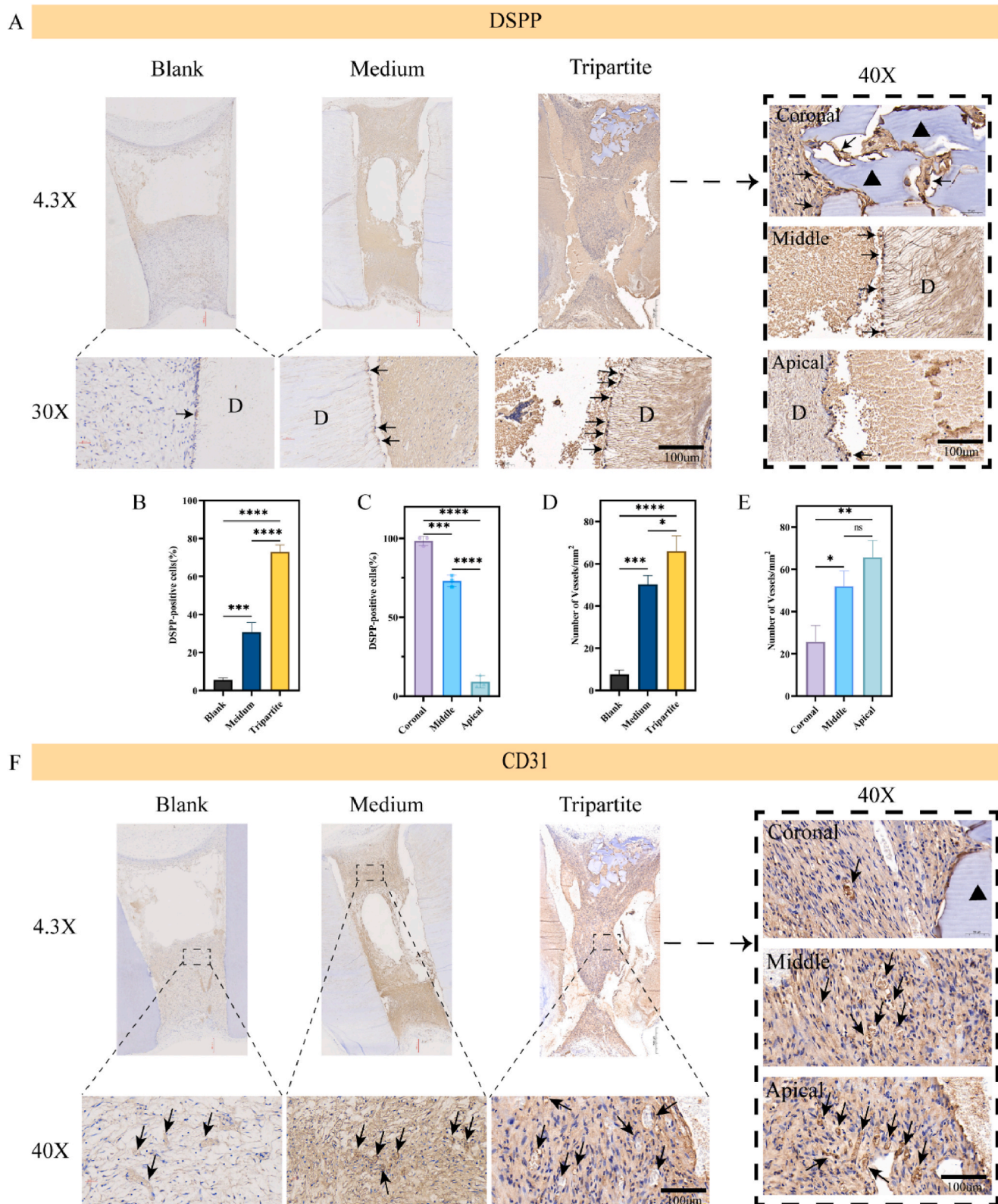


Fig. 11. Immunohistochemistry of pulp-like tissue. A) DSPP immunohistochemical staining images of pulp-like tissue. The nucleus was stained blue. The brown part indicated DSPP positive. (Notes: P: pulp tissue, D: dentin, black arrow indicates odontoblastic cells, black triangle indicates new mineralized tissue, red circle indicates new blood vessels, white arrow indicates the growth direction of root tip tissue, white dotted lines indicate the root canal divisions; the scale bar were 100 µm) B-C) DSPP positive cells were quantitatively analyzed. D-E) Quantitative analysis of CD31 positive cells. F) CD31 immunohistochemical staining images in pulp tissue. The nucleus was stained blue. The brown part indicated CD31 positive. (Note: The black arrow indicated new blood vessels, and the black triangle indicated new mineralized tissue; The scale bars was 100 µm). The data were expressed as mean ± SD. Statistical significance: * $P < 0.05$, ** $P < 0.01$, *** $P < 0.001$, **** $P < 0.0001$. Tukey back testing was used after one-way analysis of variance. (For interpretation of the references to color in this figure legend, the reader is referred to the Web version of this article.)

The precise regulation of human dental pulp stem cells was great significance for dental pulp regeneration. In 2015, Yu et al. pioneered the introduction of stiffness as a critical factor in the field of dental pulp regeneration, and determined that scaffold stiffness was a key biophysical cue in regulating DPSC differentiation [31]. In this study, we further demonstrated that three-dimensional matrix stiffness was a key biophysical cue regulating HDPSCs differentiation and paracrine signaling. Specifically, a high stiffness of 24.12 kPa was found to promoted the odontogenic differentiation of HDPSCs and the formation of crown stiffness, providing a closed and sterile environment for pulp regeneration. Low stiffness (0.79 kPa) exerted on periapical resident cells by paracrine factors from HDPSCs. It promoted the ingrowth of periapical blood vessels and provided nutrients for the regeneration of root canal tissue in time. Conversely, a low stiffness of 0.79 kPa provided a physiologic matrix environment for HDPSCs and promoted pulp formation. In vivo experiments showed that the root tips of Tripartite group were more abundant in blood vessels and fibers than those of Medium group, and the experimental conclusions in vivo and in vitro were consistent. At the same time, this study found that the Tripartite group had more abundant pulp tissue in the middle of the root canal than the Medium group. The possible reasons are as follow. On the one hand, in the narrow and elongated root canal, the Medium group faced challenges in delivering nutrients and oxygen; conversely, the low stiffness hydrogel used in the Tripartite group facilitated nutrient diffusion to the middle portion [62]. On the other hand, the sole material employed in this experiment was gelatin hydrogel, which lacked effective chemical inductive factors. In the Tripartite group, the low stiffness hydrogel in the apical region promoted cellular migration from the apex into the root canal, with cell-cell interactions supporting tissue regeneration in the middle segment [63,64]. However, the precise mechanisms underlying these processes require further investigation.

The differentiation of HDPSCs into odontoblast, induced by high stiffness, was confirmed through both in vivo and in vitro studies. We speculated that the cytoskeleton of HDPSCs attached to the high stiffness matrix contract and transmit signals to the nucleus, thus affecting the regulation of nuclear transcriptional information. Combined with RNA-seq results, this process might promote the formation of dentin by lipid metabolism pathway in the early stage, and achieve dentin mineralization by reactivating osteogenic pathways such as Wnt signaling pathway in the later stage. The deficiency in this study was that RNA-seq was performed on HDPSCs only after 7 days of induction. The 7 days sequencing results had revealed the differential genes related to odontogenesis in biological processes such as BP, revealing the early possible mechanism of 3D matrix stiffness induced odontogenic differentiation of HDPSCs. However, considering that this was only the mechanism exploration of a single node in the early stage of the experiment, further exploration of the mechanism of late odontogenic differentiation in 14 or even 21 days is still warranted. The middle part of the root canal was composed of a medium stiffness matrix, 6.37 kPa, coated with HDPSCs. The human pulp stiffness measured by Ozcan, B et al. was 5.5 ± 2.8 kPa [29]. And 6.37 kPa was the matrix stiffness model most consistent with the physical pulp stiffness in this study. Endothelial differentiation of HDPSCs cells was confirmed in vitro and in vivo. At this stiffness, cell morphology stretched. We hypothesize that actin is pulled by extracellular matrix, which affects the transcription and translation of information in the nucleus. Combined with RNA-seq results, this process may be realized by vascular related pathways such as PI3K/Akt. Previous studies have shown that PI3K/Akt pathway could affect angiogenesis by regulating the expression of VEGF, eNOS and other factors [65–67]. How 3D matrix stiffness affects endothelial differentiation of HDPSCs still needs to be verified later. The root tip area was composed of a low stiffness matrix coated with HDPSCs, and 0.79 Kpa is the lowest stiffness in this model that can better maintain the hydrogel form. At this stiffness, the cells had good vitality and morphology extension. But the indexes were not optimal in promoting the odontogenic differentiation or angiogenic differentiation of HDPSCs. This suggests that the precise

regulation of matrix stiffness is needed to regulate the differentiation of HDPSCs by three-dimensional matrix stiffness. Further, the study was pleasantly surprised to find that low stiffness matrix of 0.79 Kpa could act on periapical cells through paracrine action of HDPSCs. The low stiffness had more effects in promoting the transformation of THP-1 macrophages cells into anti-inflammatory cells, the angiogenesis of HUVECs cells and differentiation of HSF cells into vascularized fibers. Due to the narrow pore structure of apical pores, it was crucial to promote the growth of periapical blood vessels, so we selected the low stiffness matrix with the best overall effect as the tissue regeneration material in the apical region. In this work, we clarified the relationship between 3D matrix stiffness and HDPSCs. And it helped develop a strategy for promoting pulp regeneration with at Tri-Phase Biomechanical Structure based on mechanical forces. However, this study has certain limitations, particularly in the design of the in vivo experimental groups. Incorporating a biphasic model would better highlight the effectiveness of the three-phase biomechanical structure. A more detailed exploration of the mechanisms by which substrate stiffness regulates HDPSCs differentiation, along with further in vivo validation, will be key directions for our future research.

5. Conclusion

In our investigation into the role of three-dimensional matrix stiffness regulating the HDPSCs behavior, we proposed a Tri-Phase Biomechanical Structure for the pulpodentin complex regeneration through in vitro and in vivo research. We found that three-dimensional matrix stiffness directly guided the lineage specification of HDPSCs. High stiffness promoted odontoblast differentiation of HDPSCs, and the stiffness matched with physiological pulp promoted the vascular differentiation of HDPSCs, while low stiffness did not have the best effect on directly promoting HDPSCs differentiation. However, it was worth noting that low stiffness played a key role in promoting the paracrine function of HDPSCs, further promoting the inward growth of periapical blood vessels. The research emphasized the importance and feasibility of microenvironment matrix stiffness on cell reaction, provided a comprehensive basis for the optimal design and preparation of bioactive materials in dental pulp tissue engineering, and had the potential to be extended to a wider range of scaffold design and application.

CRedit authorship contribution statement

Xiujuan Li: Writing – review & editing, Writing – original draft, Visualization, Software, Methodology, Formal analysis, Data curation, Conceptualization. **Yijing Xia:** Writing – review & editing, Visualization, Funding acquisition, Formal analysis, Data curation. **Zhiying Wang:** Visualization, Supervision, Formal analysis. **Ziruo Yin:** Supervision, Software, Formal analysis. **Maotao Weng:** Supervision, Software, Formal analysis. **Feng Tian:** Supervision, Funding acquisition, Formal analysis. **Jie Kang:** Supervision, Formal analysis. **Yuanjiao Li:** Supervision, Formal analysis. **Peixuan Ding:** Supervision, Formal analysis. **Xing Liu:** Supervision, Formal analysis. **Bin Zhao:** Supervision, Resources, Project administration, Funding acquisition, Formal analysis. **Lu Wang:** Writing – review & editing, Validation, Supervision, Project administration, Methodology, Investigation, Funding acquisition, Data curation.

Declaration of competing interest

The authors declare the following financial interests/personal relationships which may be considered as potential competing interests: Lu Wang has patent Title (ZH) THREE-SECTION HARDNESS GRADIENT COMPOSITE HYDROGEL AS WELL AS PREPARATION METHOD AND APPLICATION THEREOF (Application Number: 202410880636.3) pending to none. If there are other authors, they declare that they have no known competing financial interests or personal relationships that

could have appeared to influence the work reported in this paper.

Acknowledgements

This work was financially supported by the Shanxi Key R&D Planning Program (202202130501009), Four “Batches” Innovation Project of Invigorating Medical through Science and Technology of Shanxi Province (2022XM56), Basic Research Program of Shanxi Province (Free Exploration) (202203021211225, 202203021212370, 202203021212373), Scientific and Technological Innovation Programs of Higher Education Institutions in Shanxi (2020L0207, 2023L082).

Appendix B. Supplementary data

Supplementary data to this article can be found online at <https://doi.org/10.1016/j.mtbio.2025.101591>.

Data availability

Data will be made available on request.

References

- [1] P.Y.F. Wen, M.X. Chen, Y.J. Zhong, Q.Q. Dong, H.M. Wong, Global burden and inequality of dental caries, 1990 to 2019, *J. Dent. Res.* 101 (4) (2022) 392–399, <https://doi.org/10.1177/00220345211056247>.
- [2] M.A. Peres, L.M.D. Macpherson, R.J. Weyant, B. Daly, R. Venturelli, M.R. Mathur, S. Listl, R.K. Celeste, C.C. Guarnizo-Herreño, C. Kearns, H. Benzian, P. Allison, R. G. Watt, Oral diseases: a global public health challenge, *Lancet* (London, England) 394 (10194) (2019) 249–260, [https://doi.org/10.1016/s0140-6736\(19\)31146-8](https://doi.org/10.1016/s0140-6736(19)31146-8).
- [3] D. Ricucci, S. Loghin, L.N. Niu, F.R. Tay, Changes in the radicular pulp-dentine complex in healthy intact teeth and in response to deep caries or restorations: a histological and histobacteriological study, *J. Dent.* 73 (2018) 76–90, <https://doi.org/10.1016/j.jdent.2018.04.007>.
- [4] X.Y. Zou, L. Yue, Biological basis and clinical exploration of regenerative endodontic therapy, *Chin J Stomatol* 57 (1) (2022) 3–9, <https://doi.org/10.3760/cma.j.cn112144-20210928-00444>.
- [5] M.Y. Chen, K.L. Chen, C.A. Chen, F. Tayebaty, P.A. Rosenberg, L.M. Lin, Responses of immature permanent teeth with infected necrotic pulp tissue and apical periodontitis/abscess to revascularization procedures, *Int. Endod. J.* 45 (3) (2012) 294–305, <https://doi.org/10.1111/j.1365-2591.2011.01978.x>.
- [6] M. Nakashima, H. Tanaka, Pulp regenerative therapy using autologous dental pulp stem cells in a mature tooth with apical periodontitis: a case report, *J. Endod.* 50 (2) (2024) 189–195, <https://doi.org/10.1016/j.joen.2023.10.015>.
- [7] K. Iohara, M. Tominaga, H. Watanabe, M. Nakashima, Periapical bacterial disinfection is critical for dental pulp regenerative cell therapy in apical periodontitis in dogs, *Stem Cell Res. Ther.* 15 (1) (2024) 17, <https://doi.org/10.1186/s13287-023-03628-6>.
- [8] Y. Han, J. Xu, H. Chopra, Z. Zhang, N. Dubey, W.L. Dissanayake, J.E. Nör, M. C. Bottino, Injectable tissue-specific hydrogel system for pulp-dentin regeneration, *J. Dent. Res.* 103 (4) (2024) 398–408, <https://doi.org/10.1177/00220345241226649>.
- [9] T. Yang, Q. Zhang, L. Xie, R. Zhang, R. Qian, Y. Tian, G. Chen, W. Tian, hDPSC-laden GelMA microspheres fabricated using electrostatic microdroplet method for endodontic regeneration, *Materials science & engineering, C, Materials for biological applications* 121 (2021) 111850, <https://doi.org/10.1016/j.msec.2020.111850>.
- [10] J. Li, Z. Wang, J. Wang, Q. Guo, Y. Fu, Z. Dai, M. Wang, Y. Bai, X. Liu, P.R. Cooper, J. Wu, W. He, Amphiregulin regulates odontogenic differentiation of dental pulp stem cells by activation of mitogen-activated protein kinase and the phosphatidylinositol 3-kinase signaling pathways, *Stem Cell Res. Ther.* 13 (1) (2022) 304, <https://doi.org/10.1186/s13287-022-02971-4>.
- [11] N. Monteiro, G. Thrivikraman, A. Athirasala, A. Tahayeri, C.M. Franca, J. L. Ferracane, L.E. Bertassoni, Photopolymerization of cell-laden gelatin methacryloyl hydrogels using a dental curing light for regenerative dentistry, *Dent. Mater. : official publication of the Academy of Dental Materials* 34 (3) (2018) 389–399, <https://doi.org/10.1016/j.dental.2017.11.020>.
- [12] R. Ikari, K.I. Mukaisho, S. Kageyama, M. Nagasawa, S. Kubota, T. Nakayama, S. Murakami, N. Taniura, H. Tanaka, R.P. Kushima, A. Kawauchi, Differences in the central energy metabolism of cancer cells between conventional 2D and novel 3D culture systems, *Int. J. Mol. Sci.* 22 (4) (2021), <https://doi.org/10.3390/ijms22041805>.
- [13] S.M. Naqvi, L.M. McNamara, Stem cell Mechanobiology and the role of biomaterials in governing mechanotransduction and matrix production for tissue regeneration, *Front. Bioeng. Biotechnol.* 8 (2020) 597661, <https://doi.org/10.3389/fbioe.2020.597661>.
- [14] R.T. Brady, F.J. O'Brien, D.A. Hoey, Mechanically stimulated bone cells secrete paracrine factors that regulate osteoprogenitor recruitment, proliferation, and differentiation, *Biochem. Biophys. Res. Commun.* 459 (1) (2015) 118–123, <https://doi.org/10.1016/j.bbrc.2015.02.080>.
- [15] Y. Yu, Y. Leng, X. Song, J. Mu, L. Ma, L. Yin, Y. Zheng, Y. Lu, Y. Li, X. Qiu, H. Zhu, J. Li, D. Wang, Extracellular matrix stiffness regulates microvascular stability by controlling endothelial paracrine signaling to determine pericyte fate, *Arterioscler. Thromb. Vasc. Biol.* 43 (10) (2023) 1887–1899, <https://doi.org/10.1161/atvbaha.123.319119>.
- [16] H. Yang, N.M.J. Cheam, H. Cao, M.K.H. Lee, S.K. Sze, N.S. Tan, C.Y. Tay, Materials stiffness-dependent redox metabolic reprogramming of mesenchymal stem cells for secretome-based therapeutic angiogenesis, *Adv. Healthcare Mater.* 8 (20) (2019) e1900929, <https://doi.org/10.1002/adhm.201900929>.
- [17] Z. Zhuang, Y. Zhang, X. Yang, T. Yu, Y. Zhang, K. Sun, Y. Zhang, F. Cheng, L. Zhang, H. Wang, Matrix stiffness regulates the immunomodulatory effects of mesenchymal stem cells on macrophages via AP1/TSG-6 signaling pathways, *Acta Biomater.* 149 (2022) 69–81, <https://doi.org/10.1016/j.actbio.2022.07.010>.
- [18] A.E. Lee, J.G. Choi, S.H. Shi, P. He, Q.Z. Zhang, A.D. Le, DPSC-derived extracellular vesicles promote rat jawbone regeneration, *J. Dent. Res.* 102 (3) (2023) 313–321, <https://doi.org/10.1177/00220345221133716>.
- [19] B. Li, X. Xian, X. Lin, L. Huang, A. Liang, H. Jiang, Q. Gong, Hypoxia alters the proteome profile and enhances the angiogenic potential of dental pulp stem cell-derived exosomes, *Biomolecules* 12 (4) (2022), <https://doi.org/10.3390/biom12040575>.
- [20] G. Brunello, F. Zanotti, M. Trentini, I. Zanolla, E. Pishavar, V. Favero, R. Favero, L. Favero, E. Bressan, M. Bonora, S. Sivoletta, B. Zavan, Exosomes derived from dental pulp stem cells show different angiogenic and osteogenic properties in relation to the age of the donor, *Pharmaceutics* 14 (5) (2022), <https://doi.org/10.3390/pharmaceutics14050908>.
- [21] V. Ganesh, D. Seol, P.C. Gomez-Contreras, H.L. Keen, K. Shin, J.A. Martin, Exosome-based cell homing and angiogenic differentiation for dental pulp regeneration, *Int. J. Mol. Sci.* 24 (1) (2022), <https://doi.org/10.3390/ijms24010466>.
- [22] A. Gugliandolo, E. Mazzon, Dental mesenchymal stem cell secretome: an intriguing approach for neuroprotection and neuroregeneration, *Int. J. Mol. Sci.* 23 (1) (2021), <https://doi.org/10.3390/ijms23010456>.
- [23] C. Liu, F. Hu, G. Jiao, Y. Guo, P. Zhou, Y. Zhang, Z. Zhang, J. Yi, Y. You, Z. Li, H. Wang, X. Zhang, Dental pulp stem cell-derived exosomes suppress M1 macrophage polarization through the ROS-MAPK-NFκB P65 signaling pathway after spinal cord injury, *J. Nanobiotechnol.* 20 (1) (2022) 65, <https://doi.org/10.1186/s12951-022-01273-4>.
- [24] S. Hu, B. Chen, J. Zhou, F. Liu, T. Mao, J.L. Pathak, N. Watanabe, J. Li, Dental pulp stem cell-derived exosomes revitalize salivary gland epithelial cell function in NOD mice via the GPER-mediated cAMP/PKA/CREB signaling pathway, *J. Transl. Med.* 21 (1) (2023) 361, <https://doi.org/10.1186/s12967-023-04198-0>.
- [25] A.I. Van Den Bulcke, B. Bogdanov, N. De Rooze, E.H. Schacht, M. Cornelissen, H. Berghmans, Structural and rheological properties of methacrylamide modified gelatin hydrogels, *Biomacromolecules* 1 (1) (2000) 31–38, <https://doi.org/10.1021/bm990017d>.
- [26] M. Li, X. Zhang, M. Wang, Y. Wang, J. Qian, X. Xing, Z. Wang, Y. You, K. Guo, J. Chen, D. Gao, Y. Zhao, L. Zhang, R. Chen, J. Cui, Z. Ren, Activation of Piezo1 contributes to matrix stiffness-induced angiogenesis in hepatocellular carcinoma, *Cancer Commun.* 42 (11) (2022) 1162–1184, <https://doi.org/10.1002/cac2.12364>.
- [27] Y. Cao, M. Yang, R. Zhang, X. Ning, M. Zong, X. Liu, J. Li, X. Jing, B. Li, X. Wu, Carbon dot-based photo-cross-linked gelatin methacryloyl hydrogel enables dental pulp regeneration: a preliminary study, *ACS Appl. Mater. Interfaces* (2024), <https://doi.org/10.1021/acsami.4c03168>.
- [28] X. Wang, L. Ji, J. Wang, C. Liu, Matrix stiffness regulates osteoclast fate through integrin-dependent mechanotransduction, *Bioact. Mater.* 27 (2023) 138–153, <https://doi.org/10.1016/j.bioactmat.2023.03.014>.
- [29] B. Ozcan, E. Bayrak, C. Erksen, Characterization of human dental pulp tissue under oscillatory shear and compression, *J. Biomech. Eng.* 138 (6) (2016) 061006, <https://doi.org/10.1115/1.4033437>.
- [30] J. Sun, Y.T. Chan, K.W.K. Ho, L. Zhang, L. Bian, R.S. Tuan, Y. Jiang, "Slow walk" mimetic tensile loading maintains human meniscus tissue resident progenitor cells homeostasis in photocrosslinked gelatin hydrogel, *Bioact. Mater.* 25 (2023) 256–272, <https://doi.org/10.1016/j.bioactmat.2023.01.025>.
- [31] T. Qu, J. Jing, Y. Ren, C. Ma, J.Q. Feng, Q. Yu, X. Liu, Complete pulp dentin complex regeneration by modulating the stiffness of biomimetic matrix, *Acta Biomater.* 16 (2015) 60–70, <https://doi.org/10.1016/j.actbio.2015.01.029>.
- [32] Y. Qian, J. Gong, K. Lu, Y. Hong, Z. Zhu, J. Zhang, Y. Zou, F. Zhou, C. Zhang, S. Zhou, T. Gu, M. Sun, S. Wang, J. He, Y. Li, J. Lin, Y. Yuan, H. Ouyang, M. Yu, H. Wang, DLP printed hDPSC-loaded GelMA microsphere regenerates dental pulp and repairs spinal cord, *Biomaterials* 299 (2023) 122137, <https://doi.org/10.1016/j.biomaterials.2023.122137>.
- [33] A.J. Engler, S. Sen, H.L. Sweeney, D.E. Discher, Matrix elasticity directs stem cell lineage specification, *Cell* 126 (4) (2006) 677–689, <https://doi.org/10.1016/j.cell.2006.06.044>.
- [34] L.D.F. Almeida, P.S. Babo, C.R. Silva, M.T. Rodrigues, J. Hebling, R.L. Reis, M. E. Gomes, Hyaluronic acid hydrogels incorporating platelet lysate enhance human pulp cell proliferation and differentiation, *J. Mater. Sci. Mater. Med.* 29 (6) (2018) 88, <https://doi.org/10.1007/s10856-018-6088-7>.
- [35] Y. Kurotaki, N. Sakai, T. Miyazaki, M. Hosonuma, Y. Sato, A. Karakawa, M. Chatani, M. Myers, T. Suzawa, T. Negishi-Koga, R. Kamijo, A. Miyazaki, Y. Maruoka, M. Takami, Effects of lipid metabolism on mouse incisor dentinogenesis, *Sci. Rep.* 10 (1) (2020) 5102, <https://doi.org/10.1038/s41598-020-61978-0>.

- [36] X. Ye, J. Zhang, P. Yang, Hyperlipidemia induced by high-fat diet enhances dentin formation and delays dentin mineralization in mouse incisor, *J. Mol. Histol.* 47 (5) (2016) 467–474, <https://doi.org/10.1007/s10735-016-9691-2>.
- [37] L. Sirui, S. Jingjing, Y. Shuai, Y. Yanyu, G. Yuping, W. Ying, G. Runying, Z. Xue, L. Yiming, M. Hongyan, W. Meiyue, L. Mengzhe, L. Rui, Treated dentin matrix induces odontogenic differentiation of dental pulp stem cells via regulation of Wnt/ β -catenin signaling, *Bioact. Mater.* (2022), <https://doi.org/10.1016/j.bioactmat.2021.05.026>.
- [38] L. Zhou, S. Zhao, X. Xing, Effects of different signaling pathways on odontogenic differentiation of dental pulp stem cells: a review, *Front. Physiol.* 14 (2023) 1272764, <https://doi.org/10.3389/fphys.2023.1272764>.
- [39] W. Lin, S.K.H. Chow, C. Cui, C. Liu, Q. Wang, S. Chai, R.M.Y. Wong, N. Zhang, W. H. Cheung, Wnt/ β -catenin signaling pathway as an important mediator in muscle and bone crosstalk: a systematic review, *J Orthop Translat* 47 (2024) 63–73, <https://doi.org/10.1016/j.jot.2024.06.003>.
- [40] Y. Yang, Y. Lin, M. Wang, K. Yuan, Q. Wang, P. Mu, J. Du, Z. Yu, S. Yang, K. Huang, Y. Wang, H. Li, T. Tang, Targeting ferroptosis suppresses osteocyte glucolipotoxicity and alleviates diabetic osteoporosis, *Bone research* 10 (1) (2022) 26, <https://doi.org/10.1038/s41413-022-00198-w>.
- [41] J. Mou, C. Li, Q. Zheng, X. Meng, H. Tang, Research progress in tumor angiogenesis and drug resistance in breast cancer, *Cancer biology & medicine* 21 (7) (2024) 571–585, <https://doi.org/10.20892/j.issn.2095-3941.2023.0515>.
- [42] R. Huang, J. Wang, H. Chen, X. Shi, X. Wang, Y. Zhu, Z. Tan, The topography of fibrous scaffolds modulates the paracrine function of Ad-MSCs in the regeneration of skin tissues, *Biomater. Sci.* 7 (10) (2019) 4248–4259, <https://doi.org/10.1039/c9bm00939f>.
- [43] T.H. Qazi, D.J. Mooney, G.N. Duda, S. Geissler, Biomaterials that promote cell-cell interactions enhance the paracrine function of MSCs, *Biomaterials* 140 (2017) 103–114, <https://doi.org/10.1016/j.biomaterials.2017.06.019>.
- [44] J.K. Bar, A. Lis-Nawara, P.G. Grelewski, Dental pulp stem cell-derived secretome and its regenerative potential, *Int. J. Mol. Sci.* 22 (21) (2021), <https://doi.org/10.3390/ijms222112018>.
- [45] L. Yifei, L. Haisheng, W. Jing, Y. Mengyun, P. Yuan, L. Tengfei, Z. Li, L. Gaoxing, D. Jun, Engineering bacteria-activated multifunctionalized hydrogel for promoting diabetic wound healing, *Adv. Funct. Mater.* (2021), <https://doi.org/10.1002/adfm.202105749>.
- [46] J. Wang, Discussion on the common issue about regenerative endodontic treatment, apexification or apical barrier, *Chin. J. Stomatol.* 58 (11) (2023) 1097–1102, <https://doi.org/10.3760/cma.j.cn112144-20230905-00143>.
- [47] B. Li, T. Ouchi, Y. Cao, Z. Zhao, Y. Men, Dental-derived mesenchymal stem cells: state of the art, *Front. Cell Dev. Biol.* 9 (2021) 654559, <https://doi.org/10.3389/fcell.2021.654559>.
- [48] N. Kawashima, T. Okiji, T. Kosaka, H. Suda, Kinetics of macrophages and lymphoid cells during the development of experimentally induced periapical lesions in rat molars: a quantitative immunohistochemical study, *J. Endod.* 22 (6) (1996) 311–316, [https://doi.org/10.1016/s0099-2399\(96\)80266-4](https://doi.org/10.1016/s0099-2399(96)80266-4).
- [49] M. Rodrigues, N. Kosaric, C.A. Bonham, G.C. Gurtner, Wound healing: a cellular perspective, *Physiol. Rev.* 99 (1) (2019) 665–706, <https://doi.org/10.1152/physrev.00067.2017>.
- [50] Y. Xiong, B.B. Mi, Z. Lin, Y.Q. Hu, L. Yu, K.K. Zha, A.C. Panayi, T. Yu, L. Chen, Z. P. Liu, A. Patel, Q. Feng, S.H. Zhou, G.H. Liu, The role of the immune microenvironment in bone, cartilage, and soft tissue regeneration: from mechanism to therapeutic opportunity, *Military Medical Research* 9 (1) (2022) 65, <https://doi.org/10.1186/s40779-022-00426-8>.
- [51] J. Ye, Y. Yang, W. Dong, Y. Gao, Y. Meng, H. Wang, L. Li, J. Jin, M. Ji, X. Xia, X. Chen, Y. Jin, Y. Liu, Drug-free mannoseylated liposomes inhibit tumor growth by promoting the polarization of tumor-associated macrophages, *Int. J. Nanomed.* 14 (2019) 3203–3220, <https://doi.org/10.2147/ijn.S207589>.
- [52] F. Boraldi, F.D. Lofaro, S. Bonacorsi, A. Mazzilli, M. Garcia-Fernandez, D. Quagliano, The role of fibroblasts in skin homeostasis and repair, *Biomedicine* 12 (7) (2024), <https://doi.org/10.3390/biomedicine12071586>.
- [53] P. Bainbridge, Wound healing and the role of fibroblasts, *J. Wound Care* 22 (8) (2013) 410–412, <https://doi.org/10.12968/jowc.2013.22.8.407>, 407–8.
- [54] J. Adhikari, S. Dasgupta, P. Das, D.A. Gouripriya, A. Barui, P. Basak, M. Ghosh, P. Saha, Bilayer regenerated cellulose/quaternized chitosan-hyaluronic acid/collagen electrospun scaffold for potential wound healing applications, *Int. J. Biol. Macromol.* 261 (Pt 1) (2024) 129661, <https://doi.org/10.1016/j.ijbiomac.2024.129661>.
- [55] S. Yuan, X. Yang, X. Wang, J. Chen, W. Tian, B. Yang, Injectable xenogeneic dental pulp decellularized extracellular matrix hydrogel promotes functional dental pulp regeneration, *Int. J. Mol. Sci.* 24 (24) (2023), <https://doi.org/10.3390/ijms242417483>.
- [56] P.A. Fang, K. Verdelis, X. Yang, L. Lukashova, A.L. Boskey, E. Beniash, Ultrastructural organization of dentin in mice lacking dentin sialo-phosphoprotein, *Connect. Tissue Res.* 55 (Suppl 1) (2014) 92–96, <https://doi.org/10.3109/03008207.2014.923861>, 0 1.
- [57] C. Georg, A. Imad, Pathophysiology of dental caries, *Monogr. Oral Sci.* (2018), <https://doi.org/10.1159/000487826>.
- [58] P. Sang Hyuk, Y. Ling, M.L. Robert, F. Jean-Christophe, Y. Hiromichi, Inflammation of the dental pulp, *Mediat. Inflamm.* (2015), <https://doi.org/10.1155/2015/980196>.
- [59] H. Meng, L. Hu, Y. Zhou, Z. Ge, H. Wang, C.T. Wu, J. Jin, A sandwich structure of human dental pulp stem cell sheet, treated dentin matrix, and Matrigel for tooth root regeneration, *Stem Cell. Dev.* 29 (8) (2020) 521–532, <https://doi.org/10.1089/scd.2019.0162>.
- [60] G. Chen, J. Chen, B. Yang, L. Li, X. Luo, X. Zhang, L. Feng, Z. Jiang, M. Yu, W. Guo, W. Tian, Combination of aligned PLGA/Gelatin electrospun sheets, native dental pulp extracellular matrix and treated dentin matrix as substrates for tooth root regeneration, *Biomaterials* 52 (2015) 56–70, <https://doi.org/10.1016/j.biomaterials.2015.02.011>.
- [61] A. Athirasala, F. Lins, A. Tahayeri, M. Hinds, A.J. Smith, C. Sedgley, J. Ferracane, L. E. Bertassoni, A novel strategy to engineer pre-vascularized full-length dental pulp-like tissue constructs, *Sci. Rep.* 7 (1) (2017) 3323, <https://doi.org/10.1038/s41598-017-02532-3>.
- [62] Y. Yuan, Z. Qianqian, L. Shumiao, L. Jinlong, Water: the soul of hydrogels, *Prog. Mater. Sci.* (2024), <https://doi.org/10.1016/j.pmatsci.2024.101378>.
- [63] X. Liang, L. Xie, Q. Zhang, G. Wang, S. Zhang, M. Jiang, R. Zhang, T. Yang, X. Hu, Z. Yang, W. Tian, Gelatin methacryloyl-alginate core-shell microcapsules as efficient delivery platforms for prevascularized microtissues in endodontic regeneration, *Acta Biomater.* 144 (2022) 242–257, <https://doi.org/10.1016/j.actbio.2022.03.045>.
- [64] W.Y. Lai, T.H. Lee, J.X. Chen, H.Y. Ng, T.H. Huang, M.Y. Shie, Synergies of human umbilical vein endothelial cell-laden calcium silicate-activated gelatin methacrylate for accelerating 3D human dental pulp stem cell differentiation for endodontic regeneration, *Polymers* 13 (19) (2021), <https://doi.org/10.3390/polym13193301>.
- [65] Y. Xian, X. Wang, Y. Yu, X. Chen, The mechanism of EGFL7 regulating neovascularization in diabetic retinopathy through the PI3K/AKT/VEGFA pathway, *Life Sci.* 340 (2024) 122483, <https://doi.org/10.1016/j.lfs.2024.122483>.
- [66] D. Pan, L. Xu, P. Chen, L. Miao, Y. Tian, D. Shi, M. Guo, Panax Quinquefolium Saponins enhances angiogenesis in rats with diabetes and myocardial infarction, *J. Ethnopharmacol.* 319 (Pt 2) (2024) 117252, <https://doi.org/10.1016/j.jep.2023.117252>.
- [67] L. Deng, M. Hou, N. Lv, Q. Zhou, X. Hua, X. Hu, X. Ge, X. Zhu, Y. Xu, H. Yang, X. Chen, H. Liu, F. He, Melatonin-encapsulated silk fibroin electrospun nanofibers promote vascularized bone regeneration through regulation of osteogenesis-angiogenesis coupling, *Materials today. Bio* 25 (2024) 100985, <https://doi.org/10.1016/j.mtbio.2024.100985>.